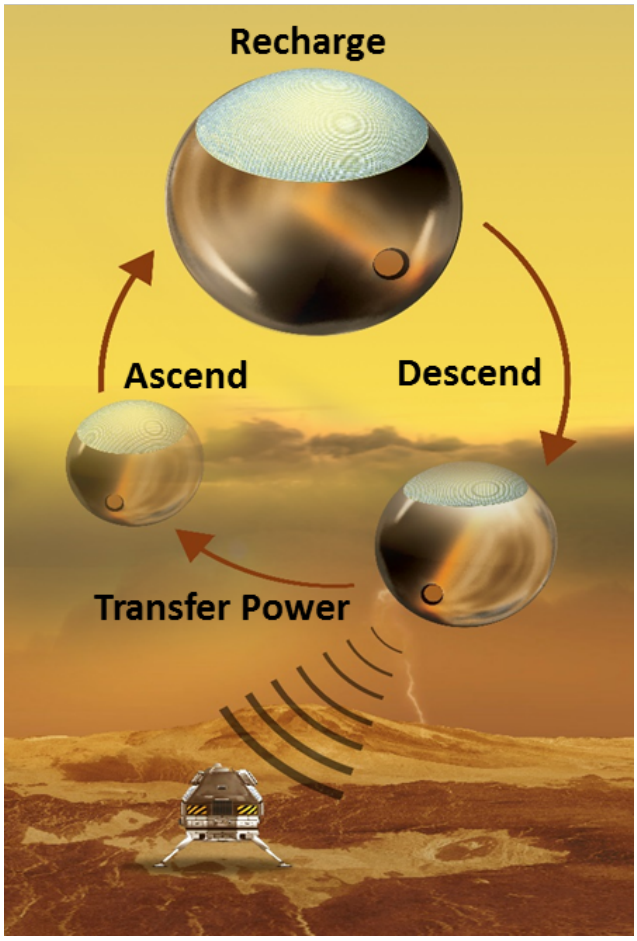

Power Beaming for Long Life Venus Surface Missions

NIAC Phase I Final Report

Erik J. Brandon, Ratnakumar Bugga, Jonathan Grandidier, Jeff L. Hall, Joel A. Schwartz and Sanjay Limaye

March 9, 2020

TABLE OF CONTENTS

1 EXECUTIVE SUMMARY AND MAJOR FINDINGS

The lack of a long-life power source capable of operating and surviving on the Venus surface fundamentally limits the *in situ* exploration of this fascinating planet. An innovative mission architecture utilizing the *wireless transfer of power* from a vehicle operating in the atmosphere of Venus to a surface lander, was evaluated and developed as part of a NASA Innovative Advanced Concepts (NIAC) Phase I study. The most promising architecture identified features a powered aircraft harvesting solar energy in the upper reaches of the Venus atmosphere using high temperature solar arrays, and storing this energy in on-board high temperature rechargeable batteries. This aerial platform would then descend below the cloud deck to transfer this energy via laser power beaming, to a lander on the Venus surface. The surface lander would include a laser power converter for receiving the beamed light energy, converting it to electrical power, and transferring it to on-board high temperature rechargeable batteries for use by the lander loads. Following this transfer of energy, the aircraft would ascend to higher altitudes, to initiate this cycle again. The option to transfer power via microwave transmission was determined to not be technically feasible, due to significant atmospheric absorption at these wavelengths. Similarly, an analysis of an architecture featuring an orbiting platform as the harvesting and beaming platform was found to not be technically feasible for the same reason. Use of balloon technology for the aerial vehicle/beaming platform showed some promise, however, this mission architecture would require multiple balloon platforms to achieve that targeted average power levels at the lander (10 W) for a 60 day mission, as well as some type of low technology readiness level control mechanism (vane or rotor) to enable overflights of the lander site. The aircraft-based concept, combined with laser power beaming, is proposed for further development in a NIAC Phase II study.

2 BACKGROUND

2.1 Venus Background

2.1.1 Venus Exploration Goals

Venus remains a priority target of interest for exploration by the space science community [1]. With its extensive cloud cover and complex atmospheric chemistry, extremely high surface temperatures and pressures, and similar size and proximity to Earth, there has been extensive speculation regarding the origins of the unique environment found on Venus. Following an extensive exploration campaign in the 1970s and early 1980s by the United States and the former Soviet Union, there has been a long hiatus without additional missions to the surface of this challenging destination. However, Venus is now warranting another look by the science community and new mission concepts are being considered. Despite some limited successes in executing landers, the enormous technical challenges associated with implementing a long-life surface mission operating at +465°C and 90 bar of atmospheric pressure still remain. The last successful lander to Venus was a Soviet mission in 1984 (Vega 2), and the last NASA mission featuring a probe that survived impact was completed in 1978 (Pioneer Multi-Probe Mission).

Venus and Earth are often characterized as “twins,” based on their very similar sizes and densities [1]. Despite these *similarities*, there are the unresolved questions that relate to their significant *differences*: the extreme temperatures, the dense carbon dioxide atmosphere and the permanent cloud coverage, the lack of oceans, and the apparent lack of plate tectonics on Venus.

The Venus exploration community is interested in resolving these key questions, to better understand the evolution of terrestrial planets. There is particular interest in using comparisons between Earth and Venus, in the search for terrestrial planets beyond our Solar System. The Venus Exploration Analysis Group (VEXAG) has developed a series of exploration goals, which include:

1. Understand atmospheric formation, evolution, and climate history on Venus
2. Determine the evolution of the surface and interior of Venus
3. Understand the nature of interior-surface-atmosphere interactions over time, including whether liquid water was ever present.

In developing a roadmap for the exploration of Venus, a notional mission concept has been developed: the Venus Flagship Design Reference Mission (VFDRM) [2]. A key element of this reference mission includes a *landed component*. A few of the top-level science questions related to a landed element include:

- Is Venus geologically active today?
- What does the surface say about Venus geological history?
- How do the surface and atmosphere interact to affect their compositions?
- What kind of basalts make up Venusian lava flows?
- Are there evolved, continental-like rocks on Venus?
- How is heat transported in the mantle, and how thick is the thermal lithosphere?
- What happened on Venus to erase 80% of its geologic history?
- Did Venus ever have oceans and, if so, for how long?

These are ultimately summarized by three main exploration themes, which include:

- What Does the Venusian Greenhouse Tell Us About Climate Change?
- How Active is Venus?
- When and Where Did the Water Go?

A common element that runs through these goals and themes is the need to perform *extended, in situ* missions on the surface of Venus, which have never been executed despite visits to Earth's twin going back as far as 1962 (by the Mariner 2 spacecraft).

2.1.2 Future Exploration Mission Concepts

To plan for a future extended mission, the Venus exploration community has highlighted the relative maturity of a variety of different technologies that could support a "simple long-life scientific probe…feasible for Venus operations" [3]. A mission involving deployment from a large platform such as Venera-D has been discussed [4], with an option to deliver a proposed Long-Lived In-Situ Solar System Explorer (LLISSE) as seen in Fig. 1 below [5]. The goal of this mission is to conduct operations for one half Venus solar day (approximately 60 Earth days), focusing on monitoring of surface winds, surface temperatures, short-term changes in atmospheric gases, and illumination during the day to night transition [6]. A key element of the mission is a long-lived seismometer, leveraging advances in high temperature electronics and sensors. Mission concept studies highlight the fact that since "there is presently no viable low-power data storage, periodic transmission of data would be needed for long-term monitoring along with a coordinated orbiter to support lander telecom," as well as the need for high temperature power sources development [3].

Fig. 1. Recent examples of Venus surface mission concepts, currently baselined using wind power generation including an Automaton Rover (left) and the LLISSE Lander (right). These landers could be powered using power beaming approaches, to address the inherent uncertainties and limits imposed by sporadic/low velocity Venus surface winds.

2.2 Limitations of Current Venus Surface Power Options

One remaining pernicious challenge in supporting a lander for any appreciable mission duration is the lack of an adequate power system, in particular viable options for surface power generation. There are current programs aimed at addressing a long-life power source for the surface of Venus, yet all have limitations that make them difficult or impossible to implement for a long life lander [7]. The potential options for power generation include: high temperature primary batteries, solar arrays, radioisotope power systems (RPS), wind power harvesting, and chemical heat sources, which are discussed below.

2.2.1 Primary and Rechargeable Batteries

Prior Venus surface missions (such as the NASA Pioneer Probes) relied on primary batteries only, which survived for approximately two hours [8]. Several surface mission concepts (Venus Intrepid Tessera Lander, or VITAL, and the Venus Mobile Explorer, or VME) feature Li/SO_2 primary batteries as the sole power source, which cannot survive Venus surface temperatures and are limited to the fixed capacity in the battery cells since they are not re-chargeable [9,10]. The use of a *non-rechargeable primary power system that is inherently unstable at high temperatures* fundamentally limits both the lifetime of a landed mission as well as the science payload, due to the required thermal management and limited energy content. Even though there are possible technological solutions for high temperature rechargeable batteries, *a power generation source to charge them is currently lacking*. The NASA High Operating Temperature Technology (HOTTech) program is currently funding efforts in the area of high temperature primary and rechargeable batteries [7,11].

2.2.2 Solar Arrays

The solar spectrum in the Venus atmosphere is different from that on Earth and varies significantly with altitude. Absorption and scattering by the atmosphere and thick cloud structure [12] reduces the intensity from ~2622 W/m^2 above the atmosphere to <100 W/m^2 at the surface. This was measured by the two Soviet descent probes, Venera 11 [13] and Venera 13 [14], which recorded the spectrally dependent downward solar radiation at altitudes between 62 km and the surface. Fig. 2 depicts the Venus atmospheric structure with three layers of clouds [15]. The solar

flux was calculated based on the Venera 11 measurements (solar zenith angle 17°). The downward solar flux is a strong function of both solar zenith angle and cloud opacity.

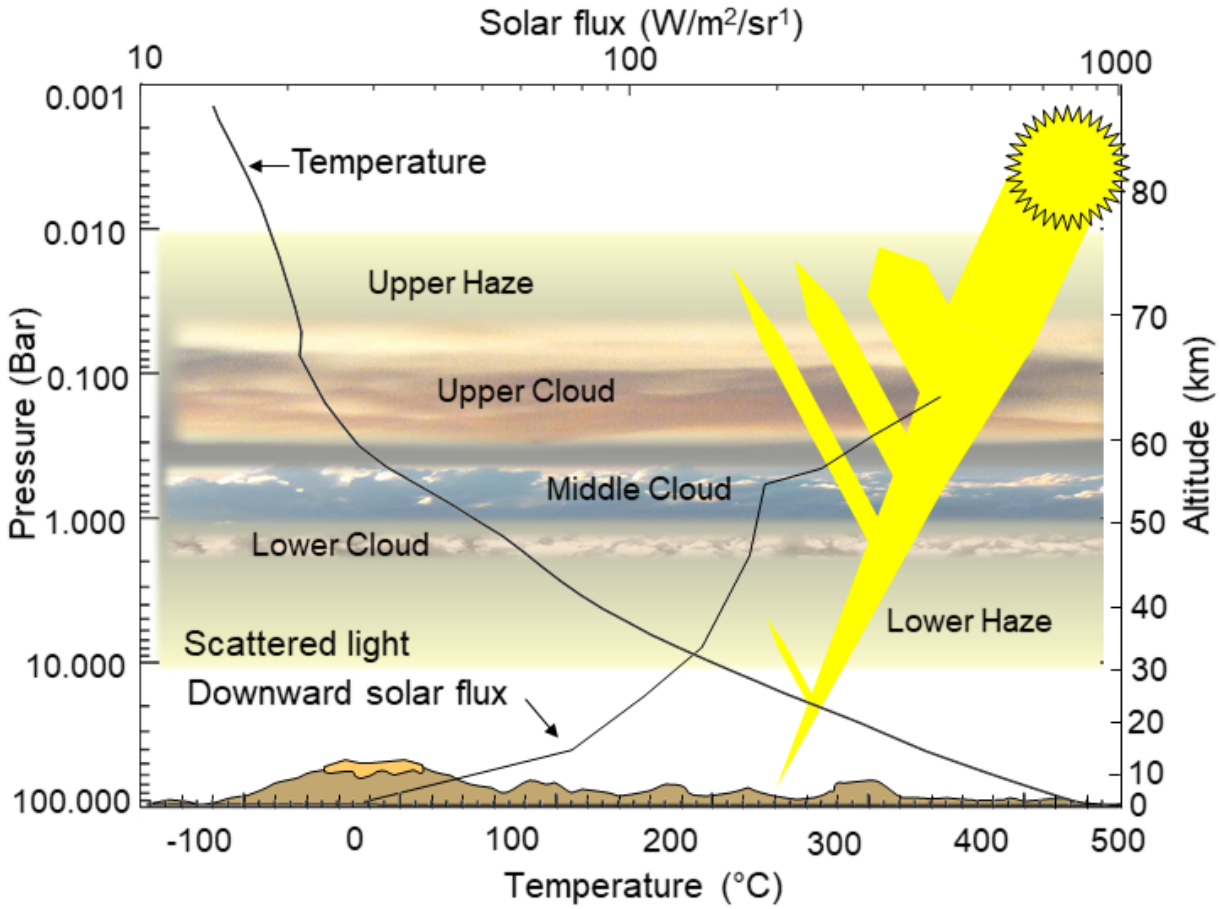

Fig. 2. Schematic of the Venus atmosphere. Temperature, pressure, and solar flux are represented. Solar flux was measured by Venera 11 (solar zenith angle 17°) [15].

Fig. 3 represents the specific power (in W/kg) of a solar array in the Venus atmosphere as a function of altitude. Direct solar radiation can be neglected at altitudes below 60 km [16] and upward solar flux is significant. For specific power calculations between the surface and 60 km altitude, a double-sided solar array mounted on both side of the solar array structure was assumed. The efficiency of the solar cell depends on temperature and impinging solar flux. Specific power was calculated based on the model described in [15,17] accounting for the isotropic nature of sunlight. Above 60 km, a conventional approach with a solar array facing up and a photovoltaic efficiency of 32% was used. These observations point to the usefulness of high temperature solar array technology at higher altitudes, despite the lack of significant insolation on the surface.

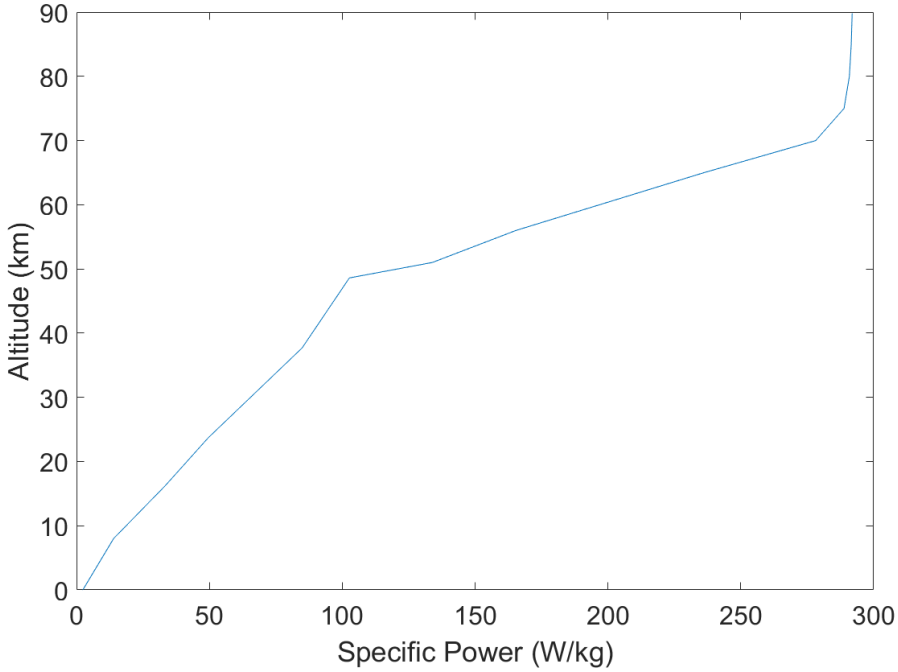

Fig. 3. Specific power (electrical power output per unit mass) of a solar array in the Venus atmosphere.

2.2.3 Radioisotope Power Sources

Radioisotope power systems (RPS), or in particular radioisotope thermoelectric generators (RTGs), have proven critical in supporting deep space fly-by and orbiter missions such as Voyager and Galileo, and planetary surface missions such as the Viking Landers and the Mars Science Laboratory. In the case of an RTG, a radioisotope heat source (plutonium-238) is used with power-generating thermocouples featuring thermoelectric materials designed for extended high temperature operation. In the latter cases, these RTGs were paired with rechargeable nickel-cadmium batteries, or recently with lithium-ion batteries, to support load leveling and high-power operations. In each of these cases, the RTG system was designed to operate in a very specific temperature regime. The hot side of the power generating thermocouples operates in the 550-1000^{0}C range (depending on the specific thermocouple material used), with the cold side rejecting heat to either the vacuum of space, or the specific planetary atmosphere where it is operating (e.g., Mars).

The current NASA option, the Multi-Mission Radioisotope Thermoelectric Generator, can ultimately be configured to operate in a vacuum or in a planetary atmosphere. All aspects of the RTG design (structure, thermal materials, thermocouples, etc.) are optimized for a specific environment (in the above cases, all at low ambient temperatures). Although operation in a high temperature, high pressure carbon dioxide environment such as Venus is technically possible [18], it would require a complete redesign of the RTG system to address operation in this challenging environment.

The environment would pose a temperature differential unlike any previously experienced by an RTG system. Use of a dynamic converter technology (i.e., Stirling, Brayton engines) is also

possible. However, the cost associated with such an extensive re-design and qualification of the heat source and converter technologies to serve a niche destination and environment such as Venus would be prohibitive, and would be accompanied by a loss of the multi-mission benefit of the current RTG technology.

2.2.4 Wind Energy

Some mission concepts [5,19-21] feature proposed harvesting of wind energy for power generation, at the surface of Venus. However, the velocity of these winds is very uncertain and likely to be too low (~2 m/s) or too sporadic to support a long-life surface lander architecture [22]. There is a finite probability of wind speeds approaching 0 m/s, in which case no power is generated. Given the critical nature of the power system to mission success, it is unlikely that a mission could be built around such a scenario. Another concern is the effect of wind turbines on seismic monitoring [23], which is a key goal of a long-life lander.

2.2.5 Other Approaches

There is also current work on "chemical" heat sources involving reaction of highly exothermic fuel/oxidizer combinations, which can be used in place of radioisotope heat sources based on plutonium-238, to power either an RTG or a dynamic RPS [24]. Although these systems show promise for replacing the plutonium-238 used (and thereby sidestepping the regulatory and cost challenges associated with their implementation), they are essentially a primary power source limited by the mass of the carried fuel and/or oxidizer. Similar approaches involving reaction of an electro-active species (such as lithium) with atmospheric carbon dioxide to form a type of "gas battery" would suffer from the same limitations [8].

3 Power Beaming Approach and Required Technology Elements

3.1 Advantages of Power Beaming

Power beaming is a method for taking a source of energy that is abundant in one location, and transferring this energy through space to a region where it is less abundant [25-30]. Conventional implementations of space-based power beaming envision transfer from a geo-stationary platform (where the attenuation of solar insolation from the atmosphere is lower than on the surface) to a stationary receiving station on the ground, to support transfer of kW or even MW of power. However, there are smaller scale concepts for power beaming on Earth, for example from the ground to an un-crewed aerial vehicle (UAV) [30]. The situation with Venus exploration represents a potentially ideal circumstance for implementation of power beaming. Solar energy is abundant in the upper reaches of the atmosphere (even greater than on or above Earth), and is highly restricted on the surface due to the extensive and persistent cloud cover.

3.2 Description of Approach and Potential Architectures

An ideal Venus-based mission architecture would involve beaming power from a Venus-stationary orbiting platform in a concentrated fashion, down to the surface. With Venus located at 0.72 AU from the sun there is approximately double the solar intensity relative Earth [31]. With the ability of various space agencies to fly very large solar arrays (such as the Juno, JUICE and Europa Clipper missions to Jupiter distances), this could support the collection and transfer of high

levels of power if emerging high temperature solar cells were used. Unfortunately, there are several reasons this is not feasible, from a mission architecture perspective. First, is the challenge of the very slow rotation of Venus (6.52 km/h), resulting in a single Venus day that is equivalent to ~243 Earth days. This would place the Venus Synchronous Orbit at a distance of 925,000 km from the surface of the planet, resulting in significant beam spreading at the point the beam energy would reach a lander [31].

Second, due the dense carbon dioxide atmosphere, atmospheric attenuation of a radio frequency (rf) signal would be too great (100's of dB) to be practical, as seen in the next Section. Similarly, due to the extensive and persistent cloud layer, an optical or laser-based approach is not practical, if beaming were to occur above this layer. Therefore, the only architecture featuring power beaming that is viable must feature collection of the abundant energy above the clouds, descent to a lower altitude (taking advantage of the transport offered by the thick atmosphere) and transfer of the energy to the lander.

To guide the development of this power beaming architecture, the LISSE concept was used as the baseline lander concept [5,6]. Over the years of Venus surface lander mission studies, concepts have typically fallen into one of three categories to support operations in the extreme Venus environment: 1) landers utilizing active cooling and a pressure vessel to shield the sensitive spacecraft sub-systems and avionics [18], 2) landers that are inherently robust under these conditions (e.g., high temperature, pressure resistant electronics and systems) [5,6] or 3) a hybrid approach that combines both of these concepts [32]. Recognizing the severe energy/power penalty with respect to active cooling for extended periods, NASA is currently focusing on the LISSE concept to guide current technology development efforts, as part of the High Operating Temperature Technology (HOTTech) program [7]. The LLISSE lander is conceived as a low mass (~10 kg) lander, that would support long duration measurements on the surface of Venus (such as seismometry) for a targeted mission of 60 days. It is anticipated LLISSE would operate on approximately 10 W of power for 60 days or 14,440 Wh of total energy. With the highest performance, high temperature primary batteries (~100 Wh/kg), this would require >140 kg of batteries. This is significantly larger than the total landed mass for LLISSE, confirming the need for new power systems to support longer duration Venus surface operations.

3.3 Types of Energy Transfer and Atmospheric Absorption Models

3.3.1 Microwave power beaming

Analysis of microwave beaming was performed by Dr. Alexander Akins of the Steffes Group at Georgia Tech [33]. The attenuation experienced by a microwave signal propagating from an orbital or atmospheric transmitter to a receiver on the surface of Venus can be determined via an atmospheric radiative transfer model. This model includes a discretization of the atmospheric structure derived from Pioneer Venus probe measurements and vertical profiles of the composition of microwave absorbers from atmospheric chemical models and prior observations. For Venus, this includes the bulk CO_2 atmosphere, SO_2, and H_2SO_4 vapor and aerosols. For completeness, the contribution of minor absorbers CO, OCS, and H_2O are also included in the model. From this information, the signal attenuation, or optical depth, of each layer in the atmosphere can be calculated using models of the microwave attenuation (in decibels per kilometer) of the relevant species developed from laboratory studies. The optical depth of a layer is computed as the layer attenuation 'k' multiplied by the layer path length 'ds.' The total optical depth τ from the surface

to a point 's' in the atmosphere is given as $\tau = \int_0^s k(s)ds$. Fig. 4 shows a contour plot of the signal attenuation in decibels from an airborne or orbital transmitter, to a surface-based receiver, as a function of transmission frequency (from 2-100 GHz) and altitude of the transmitter (from 1-100 km). The attenuation experienced by a signal transmitting from orbit is nearly the same as that transmitted from 100 km. The loss in signal strength increases with altitude and frequency, and there are no atmospheric windows in this frequency range due to the significant attenuation associated with the dense CO_2 atmosphere.

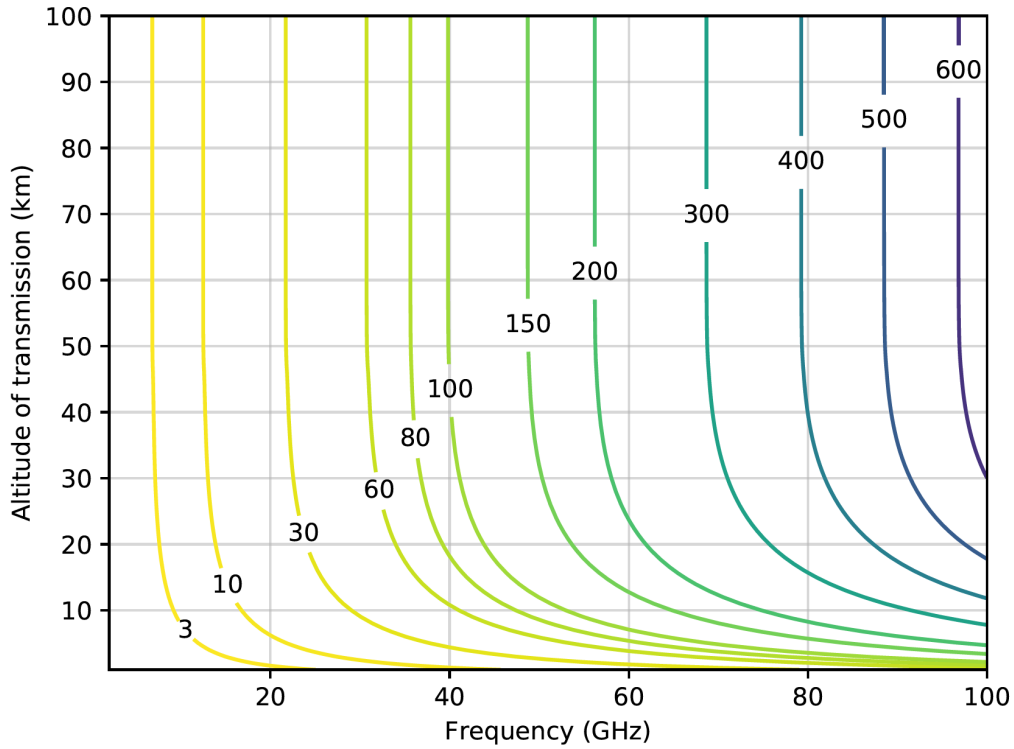

Fig. 4. Atmospheric attenuation vs. altitude and frequency for microwave power beaming, given as dB of loss [33].

3.3.2 Optical/laser power beaming

Fig. 5 was provided by David Crisp of JPL, and represents the column integrated optical depth between 0 and 102 km in the Venus atmosphere. The optical depth calculation was based on the Venus atmospheric vertical structure described in [34] and the optical properties described in [35]. The covered wavelengths are the 9200 - 9600 wavenumber range (~1041.6 - 1087 nm). This spectral range brackets the strong 1064 nm Nd:YAG line (9398.5 wavenumbers).

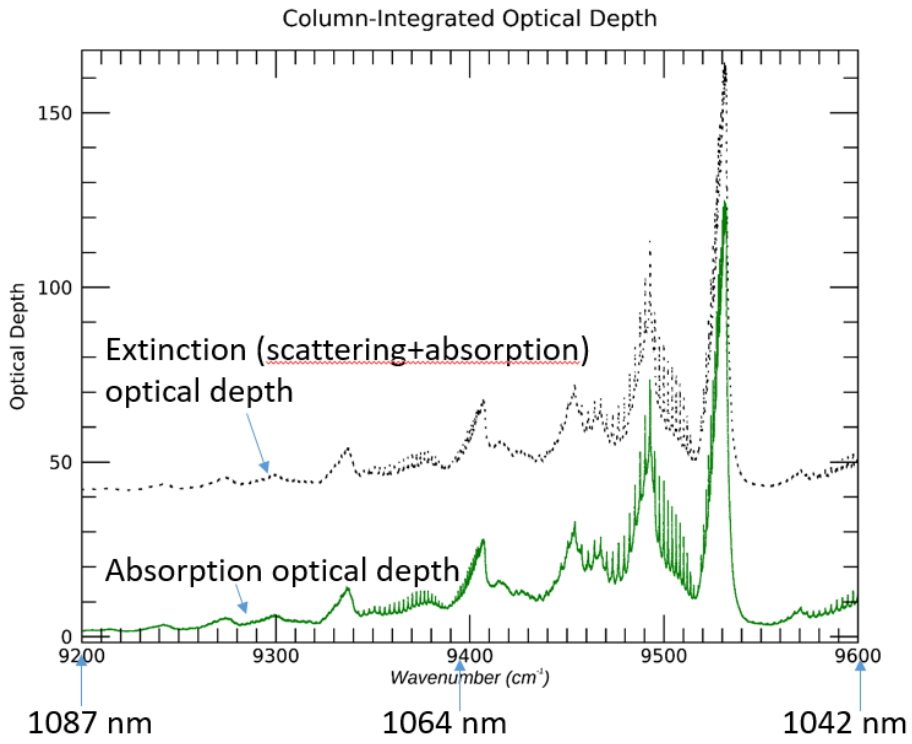

Fig. 5. Column integrated optical depth between 0 and 102 km over 50 layers. The grey dotted line corresponds to the extinction optical depth accounting for both scattering and absorption. The green line accounts for absorption only. Modelled by David Crisp (JPL).

Fig. 6 represents the extinction and absorption optical depths, between 0 and 102 km, at wavelengths of 1022 nm, 1064 nm and 1087 nm. The optical depth is the natural logarithm of the ratio of incident to transmitted radiant power through a material. For these wavelengths, absorption is low, but scattering is significant in the cloud regions above 47 km altitude. Below the base of the lower clouds, absorption becomes dominant.

The loss factor T represented in Fig. 7 was calculated per Eq. 1 as:

$$T = e^{-\tau} \tag{1}$$

where τ is the integrated optical depth over a given altitude range. As shown in Fig. 7, the loss factor decreases significantly due to scattering in the clouds. Assuming a laser beaming from below the clouds at 47 km, the transmission would be 7% at 1087 nm and negligible at 1064 nm.

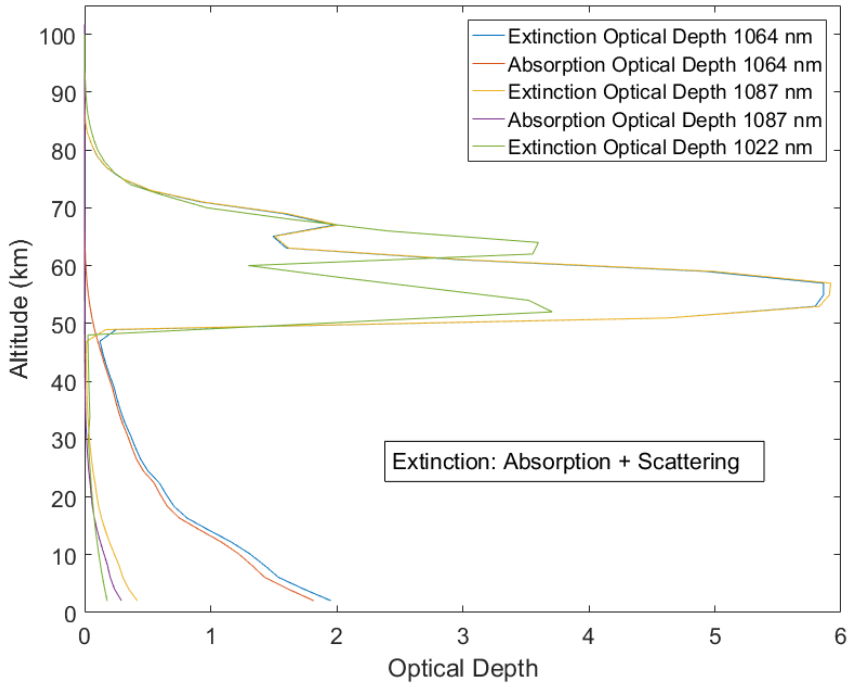

Fig. 6. Optical depths in two kilometer increments between 0 and 102 km at 1022 nm (extinction only), 1064 nm and 1087 nm (extinction and absorption). Optical depth calculations are described in Section 3.3.2. Data were provided by David Crisp (JPL) and Yeon Joo Lee (Technical University of Berlin).

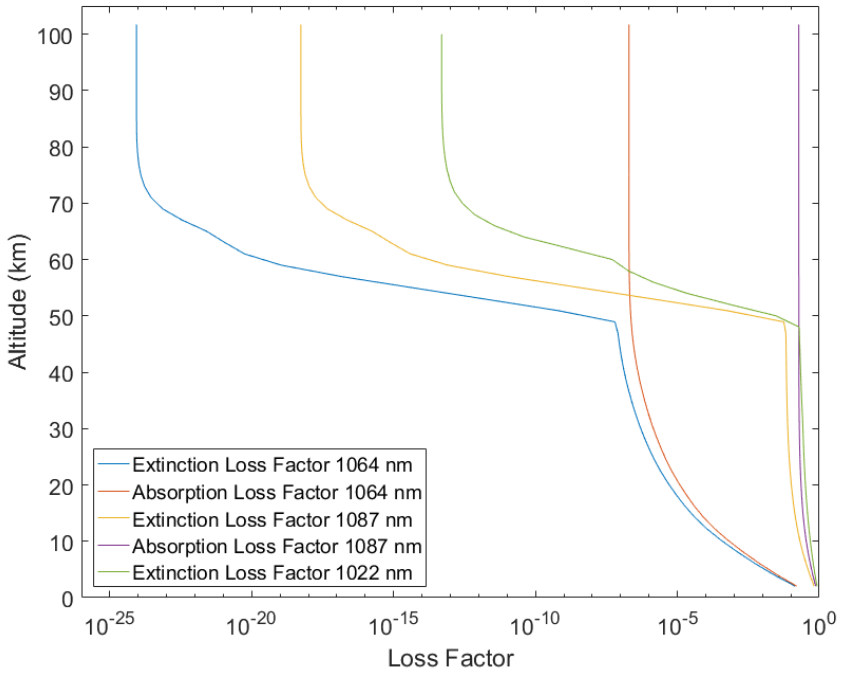

Fig. 7. Loss factor between a given altitude and the surface up to 102 km at 1022 nm (extinction only), 1064 nm and 1087 nm (Extinction and absorption). Data were provided by David Crisp (JPL) and Yeon Joo Lee (Technical University of Berlin).

Lee et al. [36, 37] modelled absorption in the Venus atmosphere for a broad wavelength range. Using that model, the loss factor between a 47 km altitude and the surface of Venus was compared. It was found that the lowest loss factor was 20% at 1022 nm, as represented in Fig. 8.

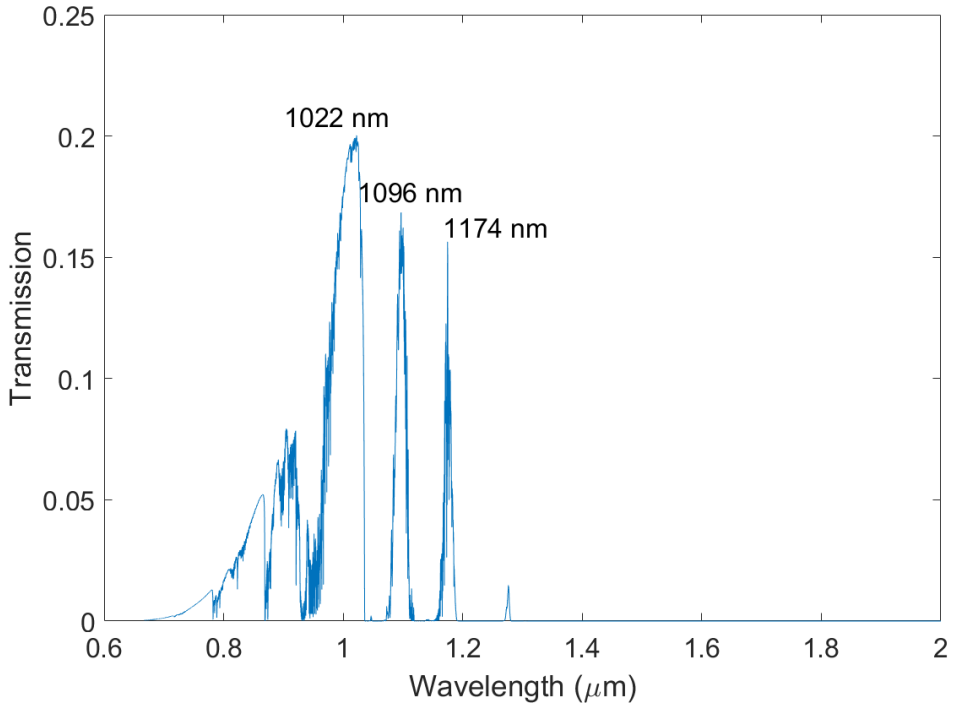

Fig. 8. Loss factor, corresponding to the transmitted light from a laser between 47 km altitude and the surface of Venus as a function of wavelength. Data were provided by Yeon Joo Lee of the Technical University of Berlin.

These observations point to a promising approach for power beaming at Venus. Short wavelength and high-power lasers in the visible and near infrared coupled with high efficiency LPCs derived from commercially available photovoltaic cells could enable power transfer (at least from an altitude below the Venus cloud deck) to the surface.

In addition to concerns over attenuation from atmospheric absorption and scattering, is the phenomena of beam spreading which is inherent to all electromagnetic radiation. This results in loss of energy if the LPC is of insufficient area to capture the incident beam, requiring a system trade between loss of efficiency vs. the added mass/volume of a larger area LPC. The beam size from a laser is limited by diffractive optics and the spot size is given approximately by Eq. 2 as:

$$d \approx \frac{2.44\lambda L}{D} \tag{2}$$

where L is the distance over which the power is beamed, λ is the laser wavelength, and D is the diameter of the laser aperture.

Based on the analysis presented in 3.3.2, the lowest loss factor between 47 km altitude and the surface of Venus is 20% for a 1022 nm wavelength. Lasers transmitting at 1064 nm are very common, due to the strong 1064 nm Nd:YAG line. However, at 1064 nm, the transmission is negligible, as presented in Fig. 8.

Ytterbium-doped fiber lasers (YDFLs) working in the near-infrared (NIR) spectral window and capable of high-power operation are currently under development. Unfortunately, the operating wavelengths of femtosecond (fs) YDFLs have mostly been confined to two spectral bands, i.e., 970-980 nm through the three-level energy transition and 1030-1100 nm through the quasi three-level energy transition, leading to a spectral gap (990-1020 nm) between these wavelengths, which is attributed to an intrinsically weak gain in this wavelength range.

In a recent paper [38], Kong et al. demonstrated a high-power mode-locked fs YDFL operating at 1010 nm, which is accomplished in a compact and cost-effective package. It exhibits superior performance in terms of both short-term and long-term stability, i.e., <0.3% (peak intensity over 2.4 μs) and <4.0% (average power over 24 hours), respectively. It is anticipated that these efforts will largely extend the capability of fs YDFLs (which are continuously tunable over the 970-1100 nm wavelength range for wideband hyperspectral operations), thus serving as a promising complement to the gold-standard Ti:sapphire fs lasers.

3.4 High Temperature Solar Arrays for Maneuverable Platform

3.4.1 Solar spectrum and intensity in the Venus atmosphere

Another key aspect of the system architecture is the solar array mounted on the maneuverable aerial platform, which harvests the incident solar radiation in the upper portion of the atmosphere. Venus atmospheric conditions are very different from Earth. Venus is a warm and dry planet. Clouds cover Venus in three layers (upper, middle and lower) between the 48 km and 68 km altitude. Sulfuric acid (H_2SO_4) is the principal constituent of the cloud particles. Clouds are surrounded by haze layers. The two descent probes Venera 11 [39] and Venera 13 [14] measured the downward solar radiation at various altitudes. Venera 11 entered the Venusian atmosphere at –14° latitude at 10:10 AM local solar time (solar zenith angle 20°) on December 25, 1978, whereas Venera 13 entered at –7.5° latitude at 9:27 AM local time (solar zenith angle 36°) on March 1, 1982 [12]. Fig. 9a shows the downward-scattered solar spectrum $F_z(\lambda)$ measured by the Venera 11 probe at various altitudes z during its descent in the Venus atmosphere and Fig. 9b compares measurements taken by Venera 11 and Venera 13 for similar altitudes. The intensity of the solar flux presented in Fig 9c is given by Eq. 3:

$$I(z) = \int_0^\infty F_z(\lambda)\, d\lambda \tag{3}$$

At a given altitude z, the intensity of the solar flux $I(z)$ was determined to be approximately 1.9 times higher for Venera 11 than for Venera 13. The solar zenith angle changes the path length by ~20%. Due to the large optical depth (see Fig. 6), that variation in path length accounts for such a large difference in solar intensity. Since Venera 11 measurements were taken closer to noon local time, these are closer to the highest solar intensity values that can be expected. At approximately 48 km, corresponding to the base of the H_2SO_4 lower cloud, a change in solar flux behavior is observed for both Venera 11 and Venera 13 (Fig. 9c).

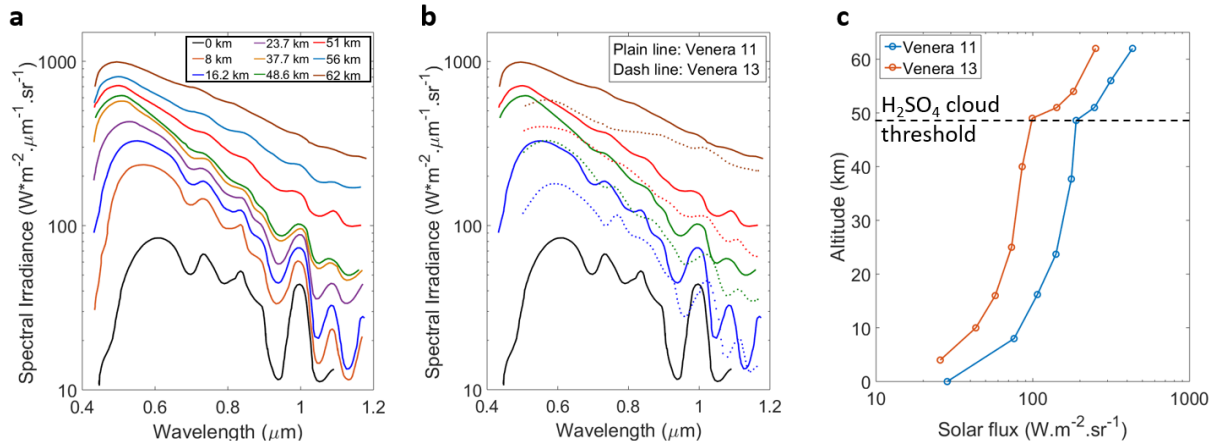

Fig. 9. (a) Solar spectra of the downward scattered solar radiation measured by the Venera 11 descent probe at various altitudes between 62 km and the surface of Venus, (b) Measurement comparison between Venera 11 (plain line) and Venera 13 (dashed line) for similar altitudes, (c) Solar flux integrated from the spectral irradiance measurements [17].

3.4.2 Attenuation and isotropic aspect of the sunlight in the Venus atmosphere

Venus orbits the Sun at a distance of 0.72 AU, and the solar intensity at Venus outside the Venus atmosphere is ~2622 W/m^2 which is about twice the Earth AM0 extra-terrestrial solar intensity (~1366 W/m^2). However, sunlight intensity is significantly attenuated within the atmosphere of Venus. Fig. 9c clearly shows this attenuation between 62 km and the surface. Due to haze and atmospheric constituents, most of the solar radiation useful for power generation is scattered [39] and direct radiation can be neglected when the altitude is less than 60 km [40]. Sunlight is isotropic below the lower clouds and the downward solar flux for a given altitude, z, can be calculated using the Lambertian distribution per Eq. 4:

$$F_D(z) = I(z) \int_0^{\frac{\pi}{2}} \int_0^{2\pi} \cos\theta \sin\theta \, d\varphi \, d\theta \tag{4}$$

Solving Eq. (4), $F_D(z) = \pi I(z)$ where $I(z)$ is the solar flux per steradian. At the surface of Venus ($z = 0$), where the temperature is 465°C and using the surface solar spectrum measured by Venera 11 (Fig. 9a), $I(0) = 28.4\ W/m^2/sr^1$ is calculated. This corresponds to a downward flux of $F_D(0) = 89.4\ W/m^2$ which is only 3.4% of the solar intensity outside the Venus atmosphere. At a 21 km altitude above the surface of Venus, where temperature is 300°C, the Venus solar spectrum was interpolated from the Venera 11 measured solar spectra. At this altitude, $I(21\ km) = 128.3\ W/m^2/sr^1$ which corresponds to a downward flux of $F_D(21\ km) = 403.1\ W/m^2$.

3.4.3 Solar Zenith angle dependence on the solar flux in Venus atmosphere

The solar flux in the Venus atmosphere strongly depends on the optical depth of the Venus clouds. The optical depth of the Venus cloud deck varies from ~25 to 45. The solar flux also depends on the solar zenith angle. Table 1 gives radiation fluxes (integrated over the spectrum) at the landing sites of five Venera stations and the Pioneer Venus large probe [40]. In addition to the directly measured values, fluxes are given adjusted to the bolometric flux ($0<\lambda<\infty$) and to a solar zenith angle of $\chi=0°$ and $\chi=45°$.

TABLE 1. Solar flux reduced to the range $0<\lambda<\infty$ and χ=Constant.

Probe	Local Flux ($0<\lambda<\infty$), W m^2	Flux (χ const), W m^2	
		$\chi=0°$	$\chi=45°$
Venera 9	95	129	73
Venera 10	60	73	41
Venera 11	78	87	49
Pioneer Venus	24.5	104	58
Venus 13	33	47	27
Venera 15	72	102	57
	Average	92±12	51±7

Due to the scattering and atmospheric conditions, the upward solar flux at Venus is very important and can be approximated, below the clouds, by $F_U(z) = F_D(z)-40$ W/m^2 [41]. Taking advantage of both downward and upward flux could increase the power density up to 69 W/m^2 at an altitude of 21 km and a temperature of 300°C. Given the nearly isotropic nature of the solar flux below an altitude of 60 km, the solar cells could be oriented at any angle. For a Venus balloon mission [42], it may be more practical to have the solar cells oriented vertically. Fig. 10 shows the power density of a solar array in the Venus atmosphere. The solar cell efficiency was calculated based on the model described earlier [15,17]. The 50 km power density is over two orders of magnitude higher than the surface value.

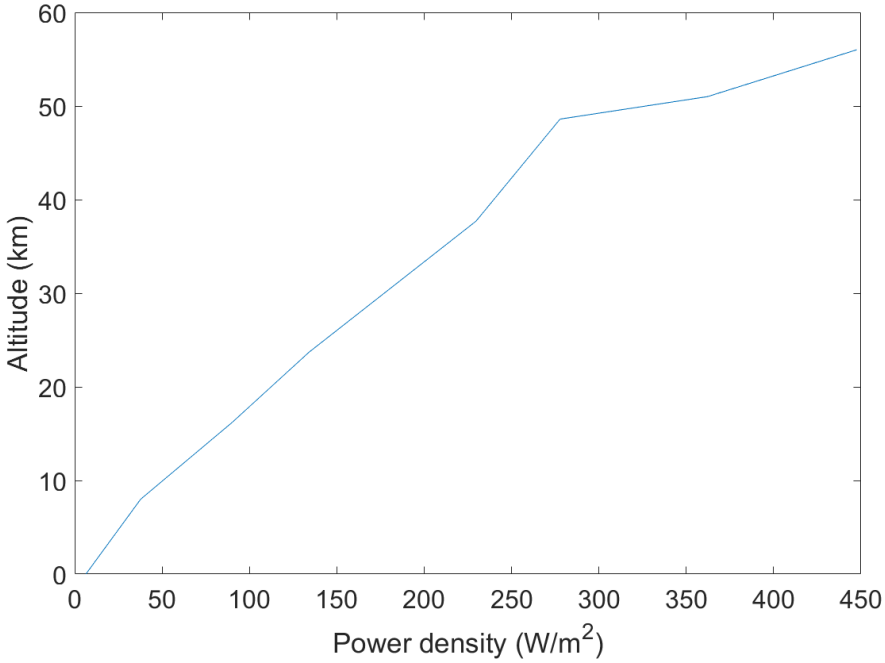

Fig. 10. Power density (electrical power output per unit area) produced by a solar array in the Venus atmosphere below 60 km altitude.

3.5 High Temperature Energy Storage Options for Maneuverable Platform and Lander

Energy storage plays a critical role in the Venus power beaming architecture; first, to store the harvested energy on the maneuverable aerial platform, and second, to store this energy on the lander, as it is beamed from this platform. The lander battery supports operations, while the aerial platform is ascending to recharge its on-board batteries. The Russian Venera series and Vega 1 and 2 Landers using conventional lithium primary batteries survived for <2 hours. Notable advances have been made at JPL in the development of high temperature primary batteries, which can provide low power levels for up to 30 days at surface temperatures [11]. For this architecture, high temperatures rechargeable batteries are needed to support extended surface missions for up to 60 days, at power levels of 10 W or more.

3.6 State of Art High Temperature Batteries

There are several high temperature rechargeable battery systems developed prior to the advent of Li-ion batteries, which operate from 250°C–400°C. This includes the LiAl-FeS_2, Na-S, and Na-metal chloride (ZEBRA) high temperature battery chemistries [8]. These batteries offer moderate high specific energies of >100 Wh/kg combined with high specific power capabilities. These batteries are well suited for long-term Venus aerial missions at low altitudes. These could be excellent candidates for the aerial platforms used for beaming power to the lander.

3.6.1 LiAl-FeS_2

The LiAl-FeS_2 system was developed extensively at Argonne National Laboratory in the early 1990s [43]. This battery employs a lithium-aluminum alloy anode (Li-Al), a mixed halide

electrolyte (LiCl+KCl) and in some cases LiBr as well, and an iron disulfide cathode (FeS_2). The operating temperature range is ~375°C–450°C, with an overall cell reaction of:

$$2LiAl + FeS_2 \Leftrightarrow Li_2FeS_2 + 2Al$$

The most advanced version employs a cylindrical, bipolar configuration with disc-shaped elements. A unit cell is comprised of discs of anode and cathode, separator, electrolyte, and inter-cell connectors. The anode is made from pressed powders of the alloy and some electrolyte. The cathode is made of pressed FeS_2 and electrolyte. The separator is made from pressed MgO powder. Even though large battery modules were reportedly built and tested for electric vehicle applications in 1980's, this technology is currently not commercially available.

3.6.2 Sodium-Sulfur (Na-S):

The Na-S system was among the first of the high temperature batteries widely studied and extensively developed, following the development of the sodium beta alumina ceramic electrolyte (with a high mobility for sodium ions at high temperatures) [44]. This battery employs a molten sodium anode, a molten sulfur cathode, and a sodium beta alumina ceramic electrolyte/separator, which has a high sodium ion conductivity of 1–10 S/cm at the operating temperatures, combined with a low electronic conductivity. The operating temperature range is 250°C–350°C. The cell has a cylindrical configuration with an outer metal case and an inner thin cylinder of the sodium beta alumina ceramic electrolyte. The sodium anode is located inside the ceramic electrolyte cylinder and partially contained within yet another thin safety can. The sulfur is contained in the annular space between the electrolyte and the outer can. A graphite-felt material and the outer can serve as the cathode current collector. This system was developed extensively for electric vehicles and even for aerospace applications, but safety problems were found to be difficult to overcome.

3.6.3 Sodium-Nickel Chloride (Na-$NiCl_2$) Batteries

This system is an improvement over the Na-S battery, with the sulfur cathode replaced with transition metal chlorides in contact with a sodium tetrachloroaluminate melt for improved safety [45-47]. This battery, pioneered in the 1980s by the Beta R&D Company and known as the "ZEBRA Battery" (Zero Emission Battery Research Activities) operates at 250°C–350°C. The cell has a cylindrical configuration with an outer metal case and an inner thin walled cylinder of the solid beta alumina ceramic electrolyte. The sodium anode is located in the annular space between the electrolyte and the metal case. The metal chloride (either $FeCl_2$ or $NiCl_2$) cathode is located inside the electrolyte tube (Fig. 11). This cathode is made of porous and partially chlorinated nickel or iron powder. A secondary molten salt electrolyte, $NaAlCl_4$, is added to the cathode material to help conduct sodium ions from the ceramic to the cathode material. The metal case serves as the anode current collector and the metallic nickel inside the cathode material serves as the positive current collector. Recently, planar Na-MCl_2 (where M indicates either Fe or Ni) is being developed with lower operating temperatures, e.g., 190°C–350°C for grid-level energy storage applications.

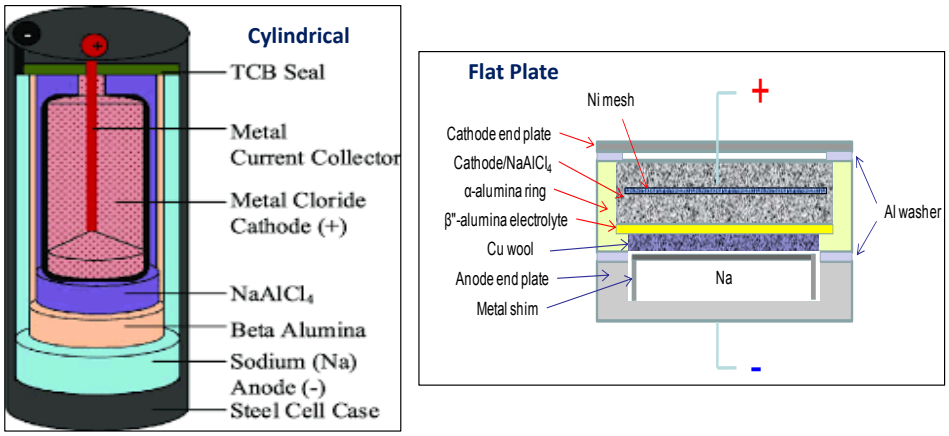

Fig. 11. Schematic view of tubular and planar Na-MCl_2 batteries.

Table 2 shows a comparison of these three high temperature battery systems. At the cell level, the specific energies of these systems are in the range of 100–180 Wh/kg, with energy densities at 150–200 Wh/L. At the battery level, the specific energies are 90-120 Wh/kg and the energy densities are 70-150 Wh/L. All of the systems offer good coulombic efficiency (near 90%) with voltage efficiencies of ~90%, yielding an overall energy efficiency of ~80% for all three options (assuming no heat losses). The cycle life of all the systems is promising for a 60 day mission architecture, where a cycle life of <200 cycles is expected (especially for the Na-MCl_2 batteries).

TABLE 2. Characteristics of high-temperatures batteries.

Characteristic	LiAl-FeS_2	Na-$NiCl_2$	Na-S
Operating Temperature Range,°C	350-400	250-350	250-350
Open Circuit Voltage, V	1.73	2.58	2.08
Theoretical Specific Energy , Wh/kg	490	800	755
Specific Energy for Cells, Wh/kg	90-130	100-130	130-180
Specific Energy for Batteries, Wh/kg	100	90-110	80-120
Energy Density for Cells, Wh/L	150-200	150-190	180
Energy Density for Batteries, Wh/L	~150	70-130	90-150
Cycle Life	>1000	>2000	2000

All three rechargeable systems have good high temperature resilience, which makes them suitable candidates for the high temperature battery used on-board the aerial energy harvesting platform (with some heating required when operating at the higher, cooler altitudes). However, they will not likely survive the Venus surface temperature of 465°C. Specifically, sodium-sulfur batteries will have the problem of increased vapor pressure from sulfur, with its boiling point (444°C) well below the Venus surface temperatures. Further, metal chloride cathodes are soluble in the molten salt electrolyte at the Venus surface temperature. The Li-FeS_2 system, on the other hand, has the problem of poor thermal stability of FeS_2 (compared to FeS), as discussed later. There is no reported performance data in literature on any these systems at temperatures beyond 400°C. As indicated, all of these are potentially suitable options for energy storage on the aerial platform, but further development is required for a rechargeable battery suitable for use on the surface of Venus.

3.6.4 Development of Batteries for Venus surface missions

Under the NASA-sponsored HOTTech project, JPL has been developing high temperature primary batteries in collaboration with an industrial partner (EaglePicher) to develop primary batteries that can survive the Venus surface temperatures of 465ºC and operate for at least 30 days to support a detailed exploration of the Venus surface [7,11]. The chemistry chosen for this battery includes: i) a lithium alloy anode (Li-Al with a melting point of 718ºC), ii) a molten salt electrolyte consisting of a eutectic mixture of lithium halides such as LiCl and KCl, which have a low melting point and high ionic conductivity, and iii) MgO as the binder, due to its non-reactivity towards lithium at elevated temperatures. Cathode materials are typically transition metal sulfides, though several other materials (including metal halides) were evaluated, with the critical criterion being their thermal stability. Iron disulfide, which is the commonly used cathode in previous high temperature batteries and current thermal batteries [8], has been shown to decompose well below the Venus surface temperatures and is unsuitable for this application.

Following thermal stability assessment, electrochemical performance was evaluated in laboratory coin cells (2032 form factor). The anode is a blend of Li-Al powder and the electrolyte powder, while the electrolyte is a blend of electrolyte powder and binder. The composite cathode features cathode active material blended with electrolyte and binder. The materials for each pellet were mixed in the appropriate ratios in an agate mortar and pestle, and pellets and were pressed at 80 MPa using a Carver hydraulic press. Laboratory test cells were assembled by stacking an anode pellet, electrolyte pellet, and cathode pellet in a standard 2032 coin cell case with a welded Ni tab. This stack was held under pressure between two Watlow 375 strip heaters using stainless steel bolts with springs to supply the pressure. Ceramic sheets were used to insulate the cells from the heaters. The cells were tested in an Ar-filled glove box. A thermocouple was inserted into one of the ceramic sheets to measure temperature. The cells were discharged using either a Bio-Logic Potentiostat VMP2 or an Arbin Battery System BT-2042 at the desired rates based on the calculated theoretical capacity of the cathode.

To verify the electrochemical activity of electrode materials, especially the cathode, cyclic voltammetry (CV) scans were carried out at the same temperature at 0.1 mV s^{-1} (Fig. 12). The FeS cathode displays only one reduction peak, beginning at 1.35V. In contrast, FeS_2 cathodes display two reduction peaks. Both the cathodes are fairly reversible, as seen from their conjugate oxidation peaks. The onset potential for oxidation for all three materials occurs at approximately 1.35V. For the FeS_2, there is also a small peak at around 1.0V; however, the origin of this peak is unclear. Based on the net charge (area under the curve) during reduction or oxidation, it appears that FeS_2 has good electrochemical activity, implying high capacity during discharge. The discharge profiles of the cells containing these cathodes at a rate of C/20 are shown in Fig. 12. The cell containing the FeS_2 has a lower capacity than the theoretical value (350 mAh/g vs. 894 mAh/g), implying that there is a loss of active material, as suggested by its poor inherent thermal stability at 475°C. The cell containing the FeS cathode, on the other hand, displays a higher discharge capacity of ~400 mAh/g, which is about 66% of its theoretical capacity. Based on its higher discharge capacity, higher (coulombic) efficiency, and better thermal stability compared to FeS_2 and MoS_2, FeS was chosen as the cathode material for further optimization studies.

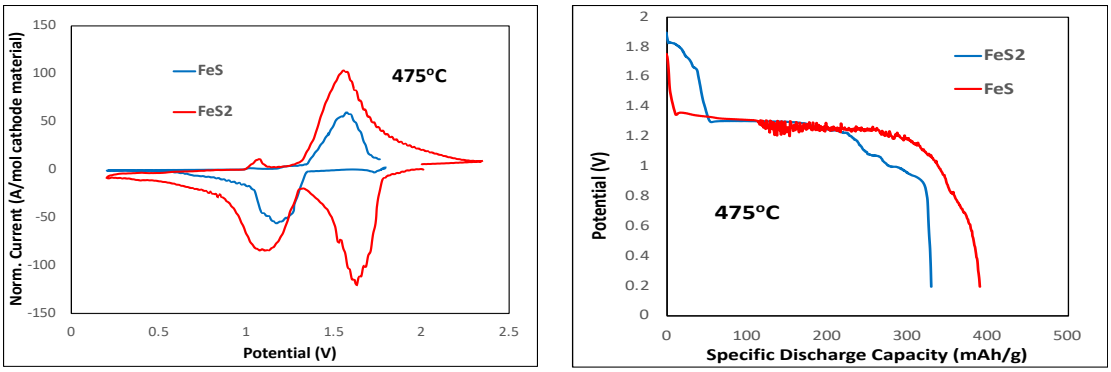

Fig. 12. Cyclic voltammetry (left) and electrochemical capacity of LiAl-FeS and LiAl-FeS_2 cells (right).

From the CV scans, it is clear that the cathode and anode processes are reversible. Fig. 13 shows the cycling of LiAl-FeS cells, after an optimization of electrolyte composition and cell design, at 475°C at moderate rate of C/20 and also at a low rate of C/720.

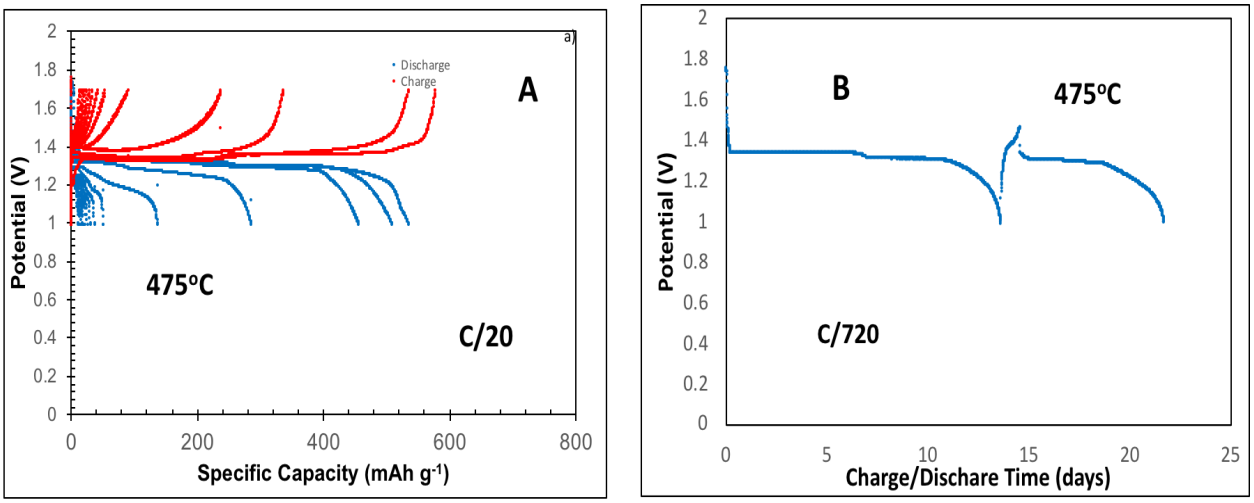

Fig. 13. Cycling of LiAl-FeS cell at a C/20 rate (left) and a low rate of C/720 (right).

As shown in the Fig. 13, the cell shows a high, near theoretical (95%) capacity at C/20 and shows good cyclability. The cell gave capacities in excess of 400 mAh/g through the first three cycles. Likewise at low rates, the cell operated over 14 days, with ~50% of capacity in the first discharge. Upon recharge, the cell operated for another 10 days. There is, however, rapid fade in capacity during cycling, which is attributed to the dissolution of the cathode into the electrolytes. This may be mitigated by using protective coatings on the cathodes, or by modifying the electrolyte. Finally, the impressive performance of the high temperature LiAl-FeS system was demonstrated in prototype cells (1.54 Ah), fabricated by EaglePicher, using modified thermal battery designs (Fig. 14).

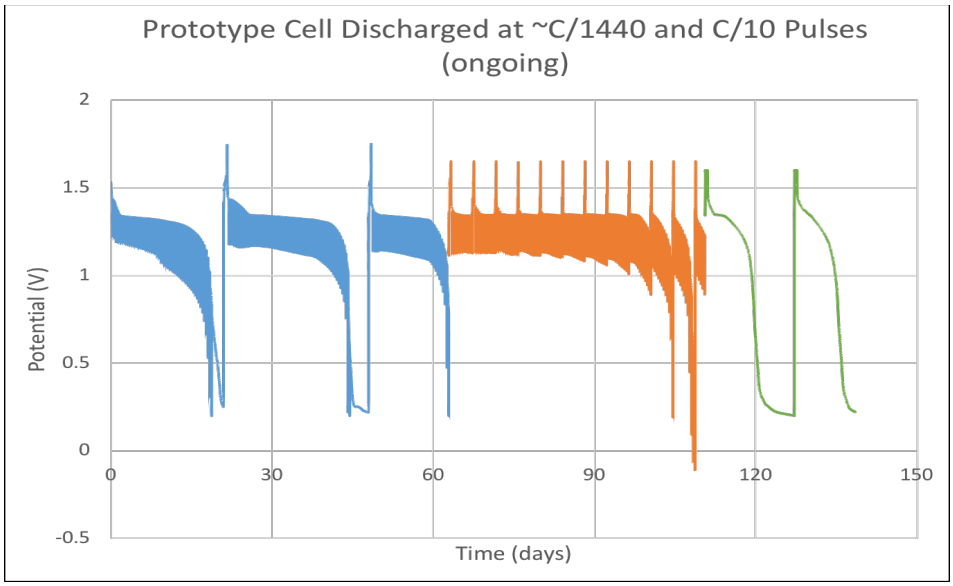

Fig. 14. Prototype LiAl-FeS cell at 475°C.

This cell chemistry was subjected to a variety of charge/discharge conditions, to establish the operating limits of the cell design. Initially, the cell was discharged at a rate of C/1440. Pulses (C/10 rate) were implemented for two minutes, after each eight hour segment, followed by charging at a C/20 rate in the first three cycles. Subsequently, the cell was recharged after 10 pulses (~10% depth of discharge). For the last two charge cycles, the cell was charged under constant current/constant voltage conditions (i.e., with a tapered current) and with no pulsing during discharge. Overall the cell operated for ~140 days at Venus surface temperatures, demonstrating the viability of this technology for long-term surface exploration missions. This technology is enabling for the proposed power beaming mission architecture, and further development of this technology is proposed for Phase II.

3.7 High Temperature Power Electronics

In addition to the main power technology elements (laser transmitter and receiver, solar arrays and high temperature batteries), high temperature electronics are required to support an end-to-end power system. In particular, the power electronics related to the power beaming transmission system are critical, and depend on the type of energy transfer selected. A comparison of the electronics needed for microwave and laser power transmission is shown in Fig. 15. Power beaming using microwave transmission would require higher frequency components. If the frequency is high enough, for example at W-band, GaN diodes would likely be needed and require development to enable operation on Venus. Development of GaN devices for this environment is underway [48,49].

In the case of laser power transmission, the power electronics would be less complex and SiC-based components would be sufficient. Power management could be accomplished using a SiC blocking diode for each photovoltaic string, and SiC switches to protect the battery from overcharge or over-discharge. SiC components for operation at Venus surface temperatures have undergone substantial development [50-52]. In the aerial platform, it is anticipated the power electronics will be at <300ºC, making commercially available high temperature technologies a

viable option. Hence, the electronics for power conversion for laser power beaming are more straightforward. In this case, the photovoltaic strings, comprising laser power converters (LPC), pose the greater challenge. Further development of the LPC is also proposed in Phase II.

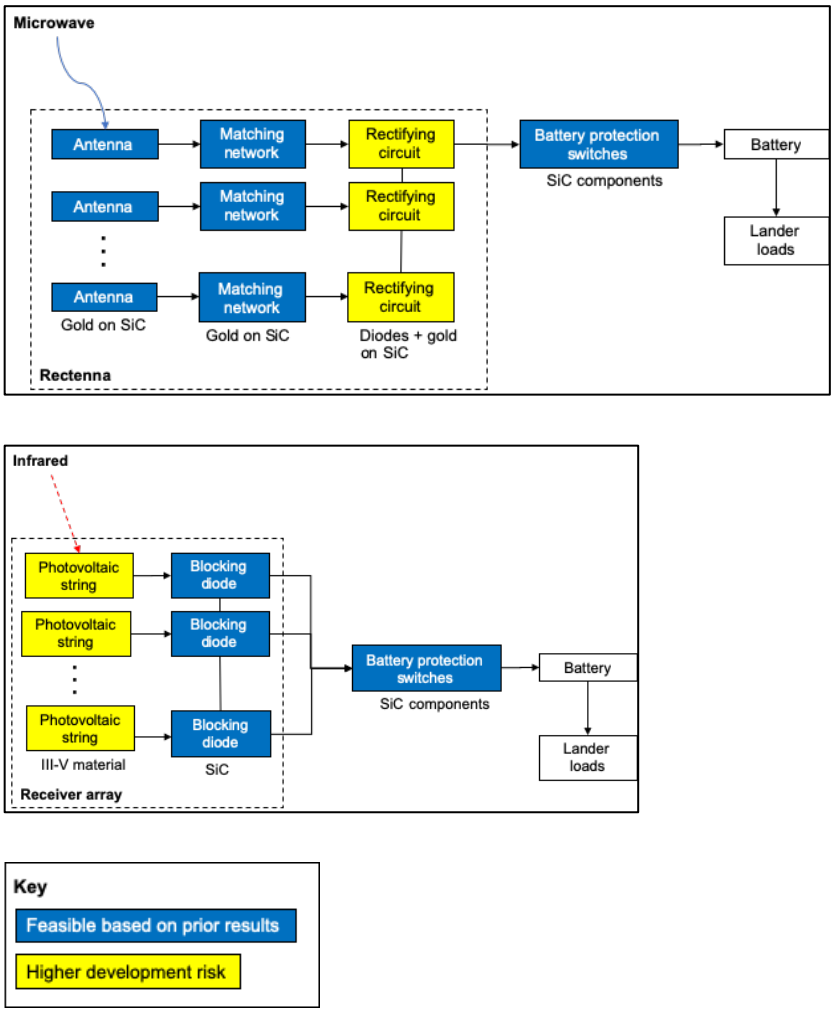

Fig 15. Lander Power Electronics. Microwave power transmission (top), would require a rectifying circuit to operate at high temperature and microwave frequencies. Laser power transmission (bottom) would utilize SiC blocking diodes and switches, but require photovoltaic strings comprising laser power converters to operate at high temperature.

3.8 Maneuverable Aerial Platforms

As part of the overall system trade studies, three types of beaming platforms were investigated, including orbiters, balloons and aircraft. An orbiting platform is potentially attractive, as it is subject to the forces of orbital mechanics only, thereby circumventing the uncertainties associated with Venus wind patterns [53]. As indicated in Section 3.2, however, implementation of an orbiting beaming platform is not feasible. This is due to the extensive absorption of rf energy by the atmosphere, or due to blocking of the surface in the case of optical/laser approaches. Therefore, much of the Phase I system study focused on the concept of a balloon platform, for harvesting and beaming energy.

The Soviet VEGA mission in 1985 demonstrated the viability of balloon flight in the Venusian clouds at an altitude of 53 km. Two helium-filled balloons were flown for 46 hours each and provided data on atmospheric conditions and winds. Despite this accomplishment, development of balloon technology for the purpose of power beaming at Venus would need to overcome a number of technical challenges not required for the VEGA mission:

- The balloon must be fabricated from high temperature compatible materials suitable for the required power beaming altitude.
- Flight duration must be increased from two days, to weeks or months.
- The balloon must have altitude control capability to move from a higher altitude where it collects and stores solar energy, to a lower altitude where it can beam that energy to the lander with minimal interference from clouds and haze.
- The balloon must incorporate some trajectory control, so that it can over fly the lander site on each circumnavigation of the planet.

JPL has assessed possible solutions to these challenges. Kapton FN is a commercially available polymer film with Teflon on one side and Kapton on the other. It is suitable for temperatures of up to ~300ºC and capable of tolerating the sulfuric acid. To use as a balloon material, it will be necessary to insert a metallization layer (vapor deposited silver) between the Teflon and Kapton layers, to reflect sunlight and minimize solar heating. This approach is feasible and is currently utilized for manufacture of thermal control blankets. A Venus balloon made from this material would be capable of operating as low as a ~15 km altitude. There is no adequate prospect for operation below this altitude, if the balloon must cycle down from the clouds. Metal balloons are possible for the high temperature below 15 km, but metal balloons are too heavy to fly above the clouds [54].

Long duration balloon flight should not be a serious challenge given the commonplace occurrence of terrestrial balloon flights for weeks and months. A more significant challenge involves integrating within the balloon *the ability to change altitude in a controllable fashion over long duration flights*. Terrestrial scientific balloons typically use ballast drops and buoyancy gas venting to control altitude, but these are finite resources that are quickly depleted. More recent approaches (e.g., Google Loon) effect altitude control with gas pumping to modulate buoyancy or weight. The recent NASA Venus Aerial Platforms Study Report [55] recognized the importance of this technology and advocated for development of a Venus balloon using this technology to achieve altitude control over long duration flights. Subsequent work at JPL [56] assessed different implementation options and quantified likely performance in terms of mass and energy consumption for a candidate mission. Adaptation of this technology may be feasible for the power beaming application, although a point design for a large altitude range (e.g., 15 to 55 km) has not yet been created.

The winds on Venus are primarily zonal. At the cloud level (50-65 km) the winds are fast with a ground relative speed ranging from 50 to 70 m/s. As a result, the balloon will be carried around the planet every 4 to 6 days. The VEGA balloons measured a small meridional component to the wind that changed the latitude; therefore, mission planners must be prepared to invoke deliberate trajectory control, to ensure overflight of the landing site on each circumnavigation. There are two basic approaches to achieve this:

- Add one or more small propellers to the balloon to impart a wind-relative flight speed to counteract the meridional wind and keep the balloon at the same latitude. Based on VEGA data the required flight speed is ~1 m/s.
- The second option is more speculative and rests on the assumption that there is structure to the Venusian winds such that the meridional winds blow northerly at one or more altitudes, and southerly at one of more altitudes. If this is true, then it is possible to vary the balloon altitude in such a way that the trajectory remains centered on the desired latitude with excursions compensated by moving to the "right" altitude. This approach is used by Google Loon to keep their balloons loitering over an area on the Earth. Whether or not Venus has this kind of wind structure is unknown, making implementation difficult.

Given the wind uncertainty with the second option, it is recommended to add propulsion to the balloon to guarantee a constant latitude flight. The required power is estimated to be ~100 W to produce a 1 m/s wind-relative speed, which is a small fraction of the total power being generated for the power beaming application itself.

Scientific balloons on Earth typically ascend at a rate of ~15 km/h when moving from the ground to the stratosphere. Similar ascent rates should be possible at Venus. However, descent rates will be slower because they are governed by the pumping ability of the variable altitude balloon [56]. Achievable descent rates will be on the order of 3-5 km/hr for reasonable pumping systems. Therefore, the payload carried by the balloon must be capable of tolerating several hours at high temperature during the descent and ascent in addition to the time spent for power beaming itself.

3.9 Description of Power System Model

A model of the power system was generated, to tie together the different technology elements and subsystems, and to enable calculations of key performance metrics, trending of performance versus design variables and overall system optimization. The model was based on the block diagram shown in Fig. 16. Two versions of the model were created, one for energy harvesting aboard aerial platforms, such as balloons, airships or aircraft [57-60] and one for energy harvesting aboard an orbiting satellite.

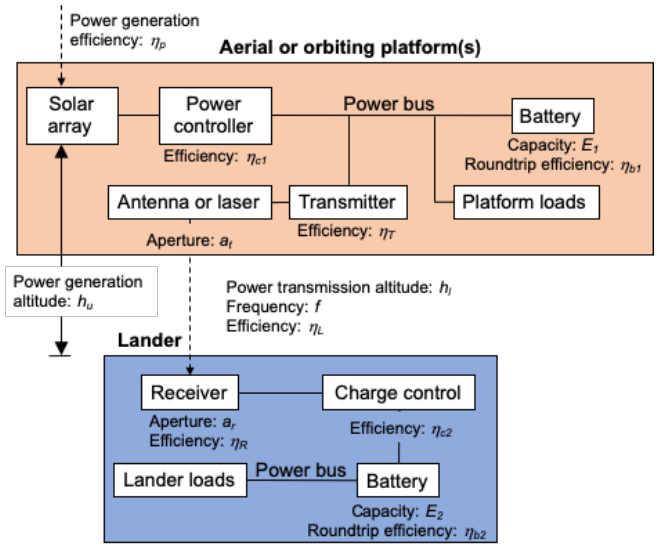

Fig. 16. Power System Block Diagram. The power system comprises power subsystems on both the lander and aerial or orbiting platforms, and transmission of power from the platform to the lander.

The overall function of the power system model is described in Fig. 17. Inputs representing the characteristics of each subsystem, referred to as "model inputs", are shown at the top. These inputs are updated as more information on each subsystem becomes available and as technology evolves. Hence, the model is intended to be used as tool to assess the impact of technology development in the future. Independent variables, listed on the lower left, represent system design parameters for the purpose of trending and optimization. These are intended to be used for trade studies (at any point during the evolution of technology), to understand the influence of architectural choices and select the preferred configuration. Key outputs of the model are shown on the lower right. These include average power available to the lander, total aerial platform mass and total lander mass.

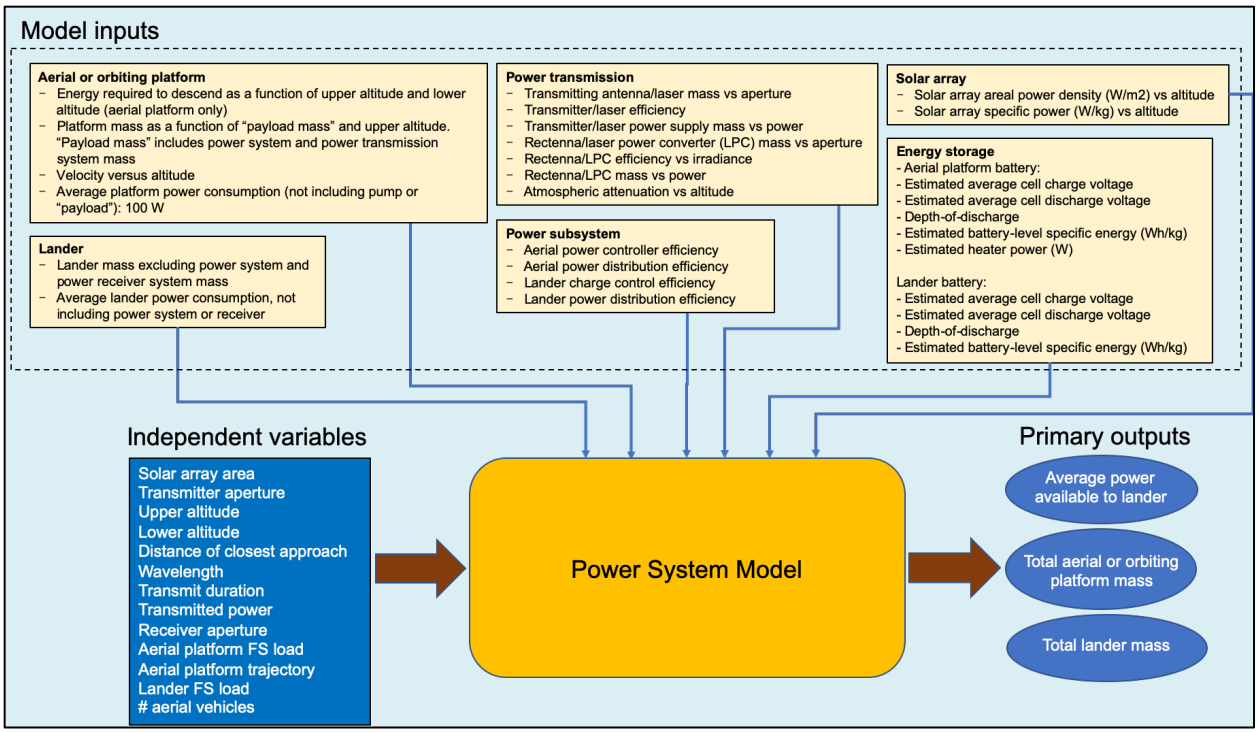

Fig. 17. Power System Model. The power system model calculates key performance metrics based on inputs from each subsystem and independent variables representing system design parameters.

A breakdown of the model structure for the case of an aerial platform is shown in Fig. 18. Each box represents an algorithm (implemented in Microsoft Excel) which takes the inputs shown and calculates the outputs shown in the figure. An iteration is performed to converge on the aerial platform mass and battery energy required to achieve the transition between upper and lower altitudes. The upper altitude is used for energy harvesting and the lower altitude is used for power transmission. The greater the platform mass, the greater the energy required for transition, which, in turn, results in greater mass. Hence, these values are iterated until they converge. Two versions of the Venus wind speed model were used, including the nominal and maximum wind speed cases [53].

The "AOI and path loss calculation" in Fig. 18 determines the effects of atmospheric losses and geometry on transmission efficiency (η_L). The acronym AOI refers to the "angle-of-incidence" of the transmitted beam on the receiving aperture. Details of the AOI and path loss calculation are provided in Fig. 19. In this calculation, atmospheric attenuation for laser transmission is derived from the optical depths provided by Y.J. Lee [36,37]. Atmospheric losses for microwaves are taken from Fig. 4 [33]. For laser power transmission, the LPC conversion efficiency (η_r) is a function of irradiance. The dependence is expected to be logarithmic and this function is modeled from the data in [17].

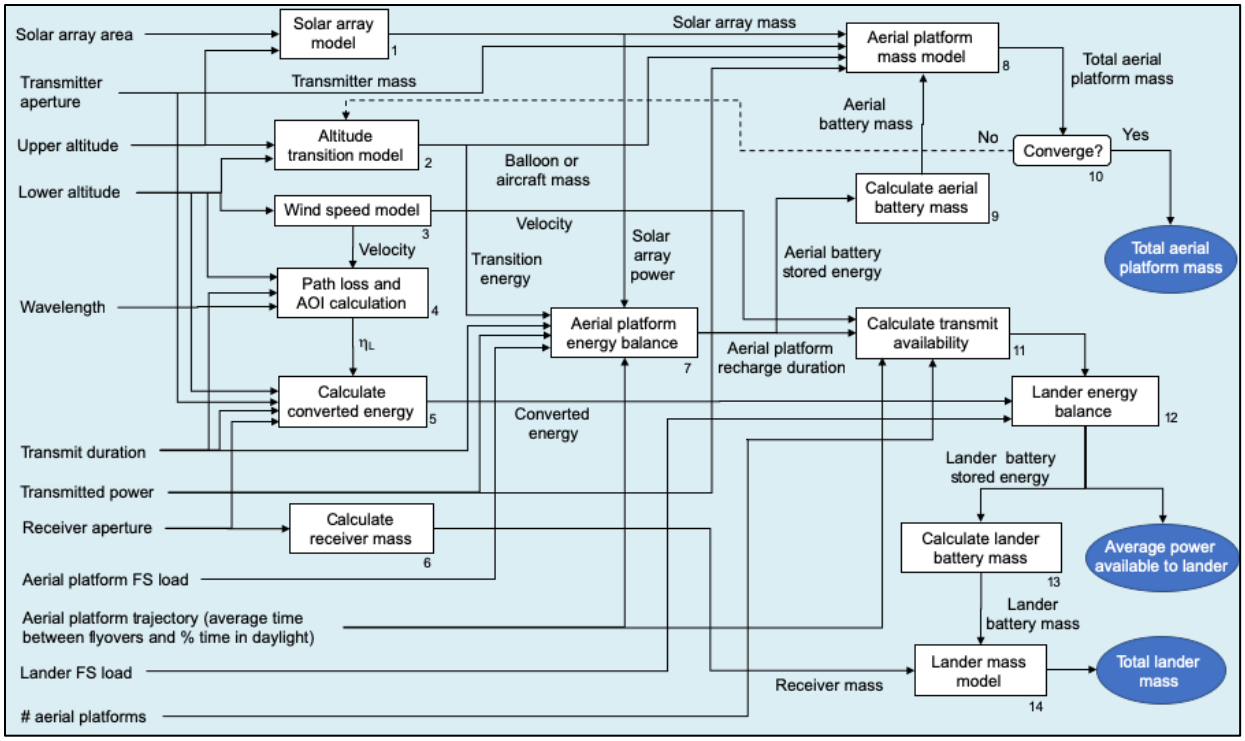

Fig. 18. Model Structure for System with Aerial Platform. Each box in the figure represents an independent algorithm. The model iterates to converge upon the platform mass and battery energy.

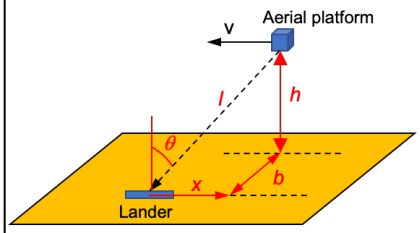

To find energy received, integrate received power over time, including four loss factors:

- ~ $1/l^2$ due to distance from source
- ~ $\cos\theta$ due to projected area of receiver
- ~ $\cos\theta$ due to projected area of transmitter (assuming no gimbal)
- ~ $e^{-l/\delta}$ atmospheric attenuation

Let P_t = transmitted power
P_r = power incident upon receiver
E_r = energy provided by receiver during period of transmission
λ = wavelength
a_t = transmitter aperture
a_r = receiver aperture
h = altitude
l = distance from lander to aerial platform
b = path offset (ground distance at closest approach)
v = aerial platform speed
$x = v(t-t_o)$ where t = time
t_o = time when x = 0
$e^{-l/\delta}$ = atmospheric attenuation factor
η_{ng} = geometric transmission efficiency at normal incidence and distance h (ignoring atmospheric attenuation)
η_r = receiver efficiency (in general, η_r is a function of P_r). For a laser power converter, we use $\eta_r(P_r) \sim a\ln(P_r/b)$ where a and b are constants.

Then, using

$$\eta_{ng} = min\left\{1, \left(\frac{\pi a_t a_r}{4h\lambda}\right)^2\right\}$$ based on antenna theory,

$$E_r = 2\int_0^{t_0} P_r \cdot \eta_r(P_r)\,dt$$

where

$$P_r(t) = P_t e^{-\sqrt{x^2+h^2+b^2}/\delta} \cdot min\left\{1, \frac{(\pi a_t a_r h)^2}{(4\lambda)^2(x^2+h^2+b^2)^2}\right\}$$

The integral E_r can be evaluated numerically.

Fig. 19. AOI and Path Loss Calculation for Aerial Platform. Effects of geometry and atmospheric losses were included in the AOI and path loss calculation.

The model for an orbiting platform is similar to the model for aerial platforms, with the following key differences. A circular orbit is assumed, as it was determined that elliptical orbits would not provide repeatable flyovers for power transmission at Venus. Since the altitude is constant, no mass or energy is required for altitude transitions and no iteration is needed to converge upon these values for the orbiter. The mass and power required for propulsion are included in the orbiter mass and energy balance models, in contrast to the model for aerial platforms. The AOI and path loss calculation for an orbiter is slightly different than the one used for aerial platforms. The curvature of the Venus surface is included and the orbiter is assumed to be above the maximum height of the atmosphere.

As discussed below (in Section 4.4), calculations showed that atmospheric losses would be overwhelming in the case of power transmission from an orbiter. For completeness, however, the model structure and details of the path loss calculation for the orbiter are provided in Fig. 20 and Fig. 21, respectively.

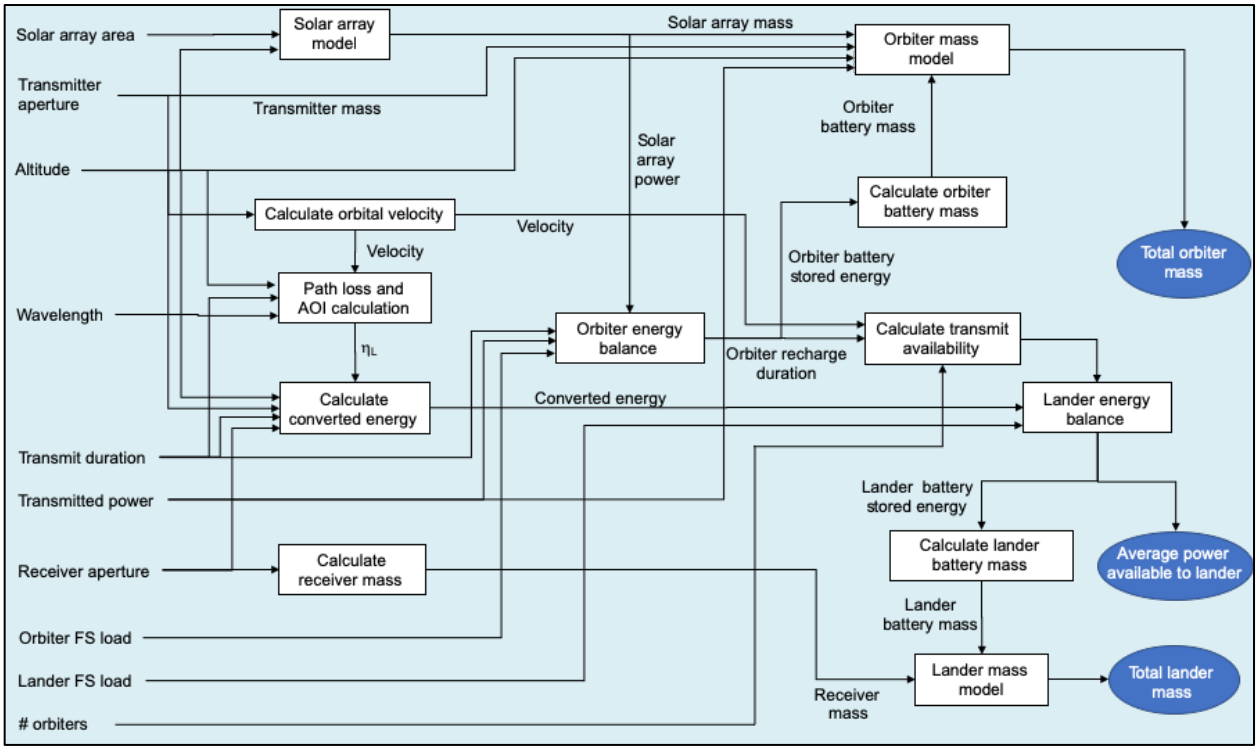

Fig. 20. Model Structure for System with Orbiting Platform. Each box in the figure represents an independent algorithm. No iteration is required to calculate the orbiter mass, but the mass needed for orbiter station-keeping is accounted for in the orbiter mass model.

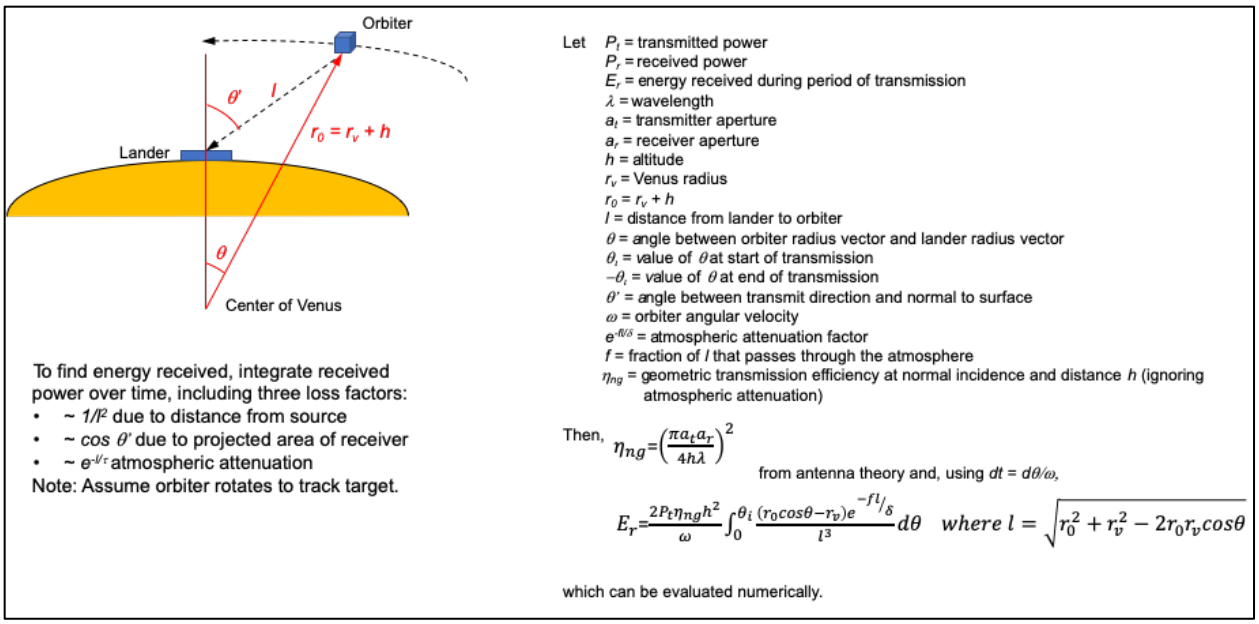

Fig. 21. AOI and Path Loss Calculation for Orbiting Platform. The calculation for orbiting platforms accounted for curvature of the surface and finite height of the atmosphere.

4 Analysis and Findings

4.1 Solar array selection and sizing

The power generated by a solar array in the Venus atmosphere strongly depends on the atmospheric conditions that vary with the altitude [15]. The solar array sizing can be approximated using Fig. 10. For example, at 47 km altitude, we can expect a power density of 271 W/m^2. Therefore, to generate 1 kW of power, a solar array of 3.7 m^2 would be required.

The solar array will provide power for operating the aerial platform and charging the battery. Power transmission will occur at lower altitudes and generally rely on energy from the battery. Hence, the array must be sized to provide enough power to recharge the battery in the time available between flyovers.

As an example, the case of a powered aircraft is discussed in section 4.4.1, below. In this case, the area of the solar array is 20 m^2 and the cruise altitude is 20 km. Then, the areal power density from Fig. 10 is 112 W/m^2 and the array power output is 2.25 kW. As discussed in 4.4.1, this enables the battery to be recharged in 11.6 hours.

4.2 Energy storage selection and sizing

For the lander energy storage, a LiAl-FeS battery was selected. Sizing was based on the following assumptions:

- Operating temperature: 465ºC
- Battery-level specific energy: 80 Wh/kg
- Depth-of-discharge: 60% (based on greater than 100 and less than 5000 cycles)

- Average cell charge voltage: 1.45V
- Average cell discharge voltage: 1.30V

For example, to provide 5 W continuous power for a period of 11.6 hours (the time required for a powered aircraft to recharge and return to beam power), the stored energy and mass would be given by:

Lander battery stored energy = (11.6 hours)(5 W)/(0.6) = 97 Wh
Lander battery mass = (97 Wh)/(80 Wh/kg) = 1.2 kg

This could be accomplished, for example, using 10 battery cells in series and a cell capacity of 7.5 Ah. For the aerial platform, sodium-nickel chloride with beta-alumina solid electrolyte was selected. Sizing was based on the following assumptions:

- Operating temperature: 250-350^{o}C
- Battery-level specific energy: 90 Wh/kg
- Depth-of-discharge: 60% (based on greater than 100 and less than 5000 cycles)
- Average cell charge voltage: 2.75V
- Average cell discharge voltage: 2.30V
- Heater power: 15% of battery energy

For the aerial platform, a heater is required to keep the battery sufficiently warm and operational when the vehicle ascends to the cooler altitudes of the atmosphere during the energy harvesting portion of the operation.

As an example, the case of an aircraft that transmits 1 kW laser output is discussed in section 4.6.1. In this case, the battery is required to provide a total of 3 kW for a period of 2 hours (2 kW are estimated for the input to the laser and 1 kW is estimated to power the aircraft). The stored energy and mass would be given by:

Aircraft battery stored energy = (1.15)(2.0 hours)(3 kW)/(0.6) = 11.5 kWh
Aircraft battery mass = (11.5 kWh)/(90 Wh/kg) = 128 kg

This example is used in preliminary estimates for the aircraft-based system, provided in Section 4.4. It results in 5 W average continuous power available to the lander for science and communications. *This analysis can be used to scale energy storage sizing to other average power levels that would be available to the lander.* More detailed analysis and mission concept development are proposed for Phase II.

4.3 Laser power beaming transmitter and receiver hardware selection

For the power beaming transmitter, a 1022 nm laser would maximize power transmission between below the clouds and the surface of Venus. This type of laser is currently under development as described in 3.3.2. Fig. 22a shows the variable temperature external quantum efficiency (EQE) measurements of a GaInP (dash line)/GaAs (solid line) two junction solar cell between 25 and 300°C. The EQE could not be measured above 300°C due to the high saturation dark current. Based on Fig. 22a the bandgap of GaAs was plotted on Fig. 22b up to 300°C and was linearly extrapolated up to 465°C. The extrapolation suggests a bandgap of 1069 nm at 465°C. This makes GaAs a very good LPC candidate with a 1022 nm laser.

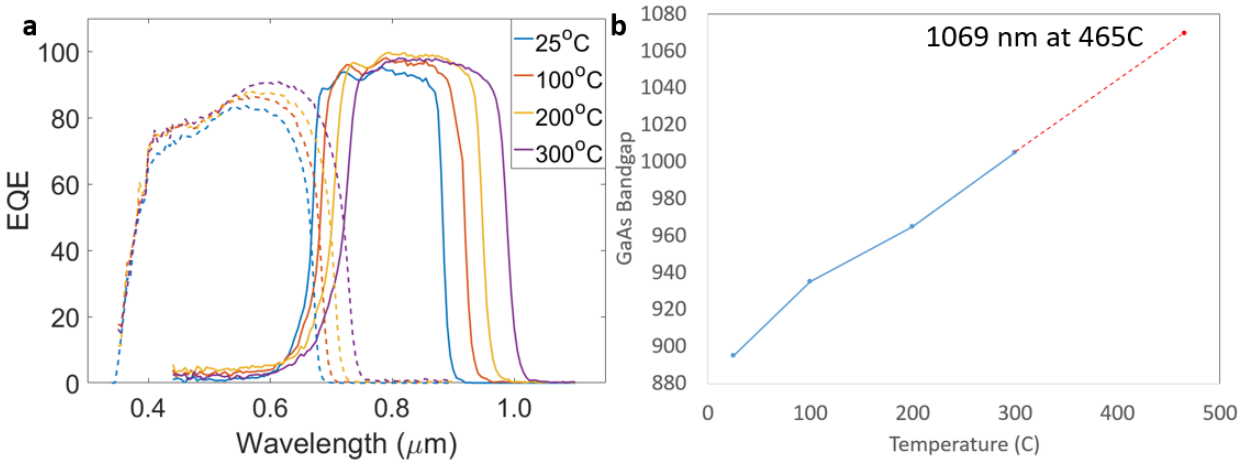

Fig. 22. a) Variable temperature EQE measurements of a GaInP (dash line)/GaAs (solid line) 2 junction solar cell between 25 and 300°C [17] and b) Bandgap of GaAs between 25 and 465°C. Above 300°C, the bandgap was extrapolated.

The estimated efficiency for a GaAs LPC at 465°C is between 5% for 100 W/m^2 and up to 10% for 1 kW/m^2. This is based on the LPC value at 25°C and the solar cell measurement at 465°C [17]. Additional modelling and high temperature measurements are needed for more accurate values, and these activities are proposed for Phase II.

4.4 Power system modeling results

Several candidate architectures were evaluated to enable power beaming to a lander on the Venus surface. These include laser power beaming from aerial platforms, microwave power beaming from aerial platforms and laser power beaming from an orbiting satellite. Laser power beaming from a fixed wing aircraft was also considered; however, aircraft mass and power consumption were not modeled as part of the Phase I task, hence, results for the aircraft are considered notional at present. A description of the power system model and calculations is provided in Section 3.9.

A summary of results is presented in Table 3. As shown in the table, laser power beaming from a polymeric balloon is preferred when compared with the other candidate options that were studied in detail. However, as discussed below, this also assumes a sufficient knowledge of local wind patterns on Venus and/or integration of an adequate trajectory control technology, which introduces new implementation challenges. Laser power beaming from an aircraft may be more advantageous than the balloon; however, more detailed study is needed, including modeling the aircraft mass and power consumption, to confirm this. Results for each architecture are described in detail below.

TABLE 3. Results Summary

Type of transmission	Energy Harvesting Platform	# of Platforms	Transmitted Power	Average Power Available to Lander	Assessment
Microwave	All	1	-	-	Not feasible
Laser	Metallic balloon	1 5	10 kW 10 kW	1.2 W 5.9 W	Feasible but less attractive than polymeric balloon
Laser	Polymeric balloon	1 5	10 kW 10 kW	2.4 W 11.8 W	Preferred
Laser	Orbiter	1	-	-	Not feasible
Laser	Aircraft (fixed wing)	1	1 kW	5 W	Requires further study in Phase II; values are notional

4.4.1 Results for laser power beaming from aerial platforms

System trades were performed for the case of an aerial platform using a balloon to control altitude. Two types of balloon were considered, polymeric and metallic. For polymeric balloons, the lowest feasible transmitting altitude was considered to be 20 km. Below this altitude, the polymeric material could not be expected to survive the atmospheric environment. For metallic balloons, the lowest feasible transmitting altitude was 10 km, because it was concluded that rapid changes in wind direction would make control of the balloon impractical at lower altitudes. In addition, the metallic balloon was constrained to cruise at a maximum altitude of 20 km, since the balloon itself would be too heavy to rise above this limit.

For both types of balloon, it was assumed that the trajectory would follow the equator and circumnavigate the planet. This is because the strong latitudinal winds would dominate navigation and a balloon would not be able to overcome these winds. It was assumed that navigation in the longitudinal direction would be possible and that the balloon could fly over the lander without significant offsets in this direction (ultimately requiring one or more of the control approaches outlined in Section 3.8, along with an adequate knowledge of the local wind patterns). The system model includes this offset as an independent variable and therefore the influence of offset can be further studied.

Trade studies enabled key system variables to be identified. Then, the average power available to the lander could be maximized. Average power and aerial battery mass for one polymeric balloon are plotted versus the transmit duration in Fig. 23. The figure shows results assuming the nominal wind speed model (at left) and the maximum wind speed model (at right). The cruise altitude is 60 km and the transmitting altitude is 20 km. In both cases, it is clear that the largest practical transmit duration is two hours. For longer durations, the improvement in available power is insignificant and the battery mass increases dramatically.

Average power and aerial battery mass for one metallic balloon are plotted versus the transmit duration in Fig. 24. The assumed cruise altitude is 20 km and the transmit altitude is 10 km. The largest practical transmit duration is again two hours. Also note that the metallic balloon provides less power to the lander, compared with the polymeric balloon, assuming the same transmit power. This result is driven by the time required for the balloon to circumnavigate the planet and return to charge the lander; the polymeric balloon, cruising at higher altitude, can circumnavigate faster.

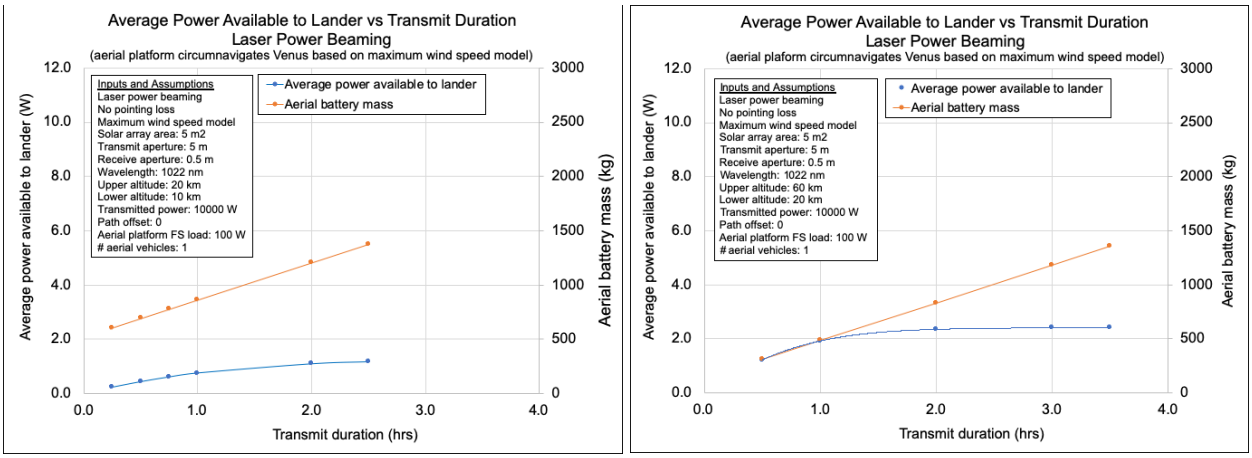

Fig. 23. Effect of Transmit Duration for Polymeric Balloon. At an altitude of 20 km, transmit durations up to 2 hours can provide useful power, for both nominal (left) and maximum (right) wind speed conditions.

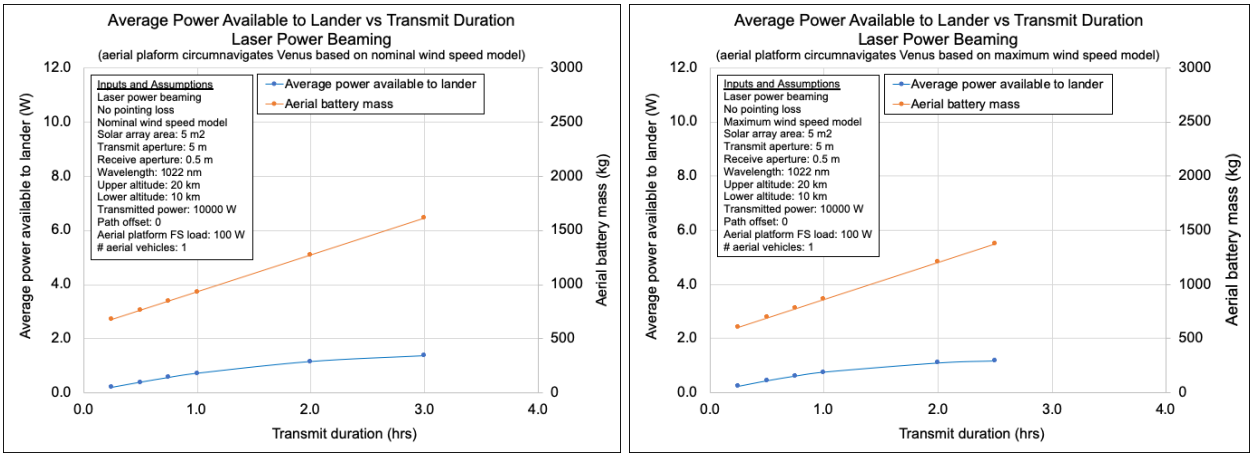

Fig. 24. Effect of Transmit Duration for Metallic Balloon. At an altitude of 10 km, transmit durations up to 2 hours can provide useful power, for both nominal (left) and maximum (right) wind speed conditions.

The effect of using multiple aerial platforms was also evaluated. Since the polymeric balloon appeared advantageous compared with the metallic balloon, emphasis was placed on this case. It was assumed that each aerial platform circumnavigates the planet above the equator. The average power available to the lander was calculated as a function of the number of aerial platforms, as shown in Fig. 25. The figure provides results assuming a cruise altitude of 60 km, a transmit altitude of 20 km and a transmit power of 10 kW.

As shown in Fig. 25, power to the lander increases linearly with the number of aerial platforms. Using the nominal wind speed model (shown at left), four platforms would be needed to achieve an average power of 10 W available to the lander. Using the maximum wind speed model, five platforms would be needed to achieve 10 W. It should be noted that the 10 W would be available continuously, through both day and night.

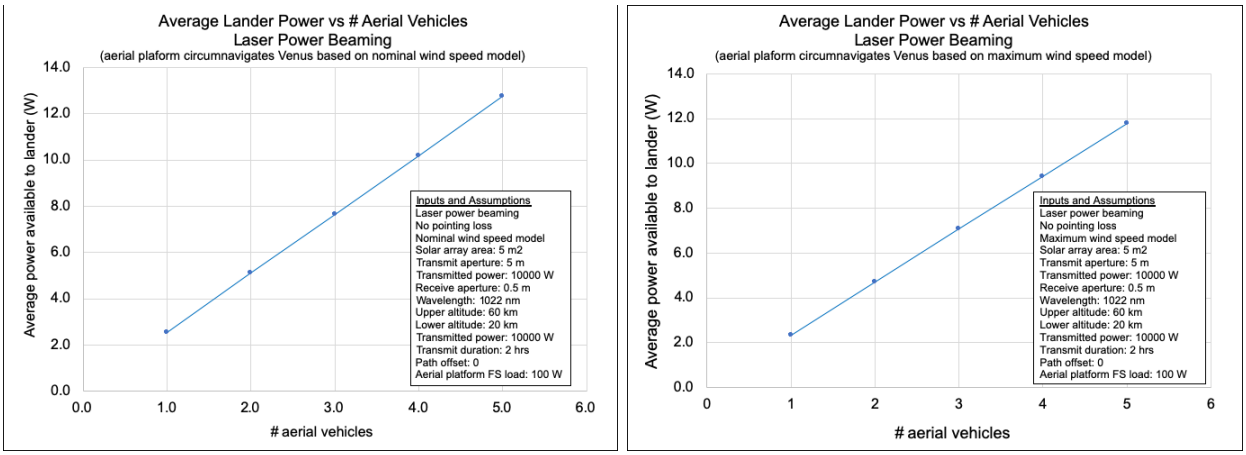

Fig. 25. Effect of Multiple Aerial Platforms. Multiple aerial platforms can be used to achieve an average power of 10 W available to the lander.

Preliminary calculations were performed for the case of an aircraft instead of a balloon. Data on aircraft mass, power consumption and energy required to transition between altitudes were not developed in Phase I, so initial calculations were performed using the following simplified assumptions:

- Aircraft mass: 400 kg
- Cruise altitude: 20 km
- Transmit altitude: 10 km
- Flight system power consumption (does not include power needed for transmission): 1000 W
- Energy required for altitude transition: TBD (initially assumed to be 0)
- Power transmitted from laser: 1000 W
- Aircraft ground speed assumed approximately equal to nominal wind speed during power transmission to lander

Likely the weakest assumption is the power required for the aircraft powered flight. The aircraft option was identified late in the Phase I studies, therefore, there was not sufficient time to fully evaluate this assumption and it is likely this number will grow. There are several unknowns, in particular the amount of power required to fly against the wind of Venus at the lower altitudes (for station-keeping), as well as to transition from lower to higher altitudes. Although these values require further study and refinement during Phase II, this aircraft mass is very similar to that proposed in the Venus Aerial Maneuverable Platform (VAMP) concept, by Northrup-Grumman [57]. VAMP is a hybrid vehicle that gets most of its lift from buoyancy and only some from aerodynamics The VAMP concept contemplates aircraft in the 90 to 880 kg range. This concept may be difficult to implement, however, at higher temperature and higher wind speeds. If this is the case, two or more lower mass aircraft (a fractionated approach, similar to the balloon concept) could be employed as part of the overall mission architecture to reduce its size and provide for redundancy.

Preliminary results for a single aircraft are shown in Fig. 26. Specifically, average power available to the lander is plotted versus the time between flyovers (from the beginning of one flyover to the beginning of the next flyover). The aircraft has the advantage that it can return to transmit power much sooner than the balloon, since it does not necessarily need to circumnavigate

the planet. For the initial case shown in Fig. 23, it can return after only 11.6 hours. However, further study is needed to determine if circumnavigation can be avoided with an aircraft, which would decrease the average power levels available at the lander (or require multiple aircraft). Of particular concern is the power required for a "station keeping" approach (i.e., flying in a circular path for energy harvesting and beaming), as well was the required methods for aircraft control at a particular altitude. In contrast, for the polymeric and metallic balloon cases in Fig. 23 and Fig. 24, at nominal wind speed, the balloon returns after 133 hours and 688 hours, respectively. In this case, the average power available to the lander for science and communications is 5 W. Table 4 provides a summary of the energy balance preliminary analysis for the lander, showing the various losses that contribute to the net available power.

Based on the advantage in navigation provided by the aircraft, further analysis is proposed for the Phase II effort. For example, in Fig. 26, the minimum time between flyovers is determined by the time required to recharge the battery. This can be increased by using a larger solar array, potentially increasing the power available to the lander. To further investigate the aircraft approach, the input assumptions will need to be refined. Specifically, the mass, power, altitude transition energy and constraints on size and flight path will need to be studied for the aircraft, and then used as inputs to the system model.

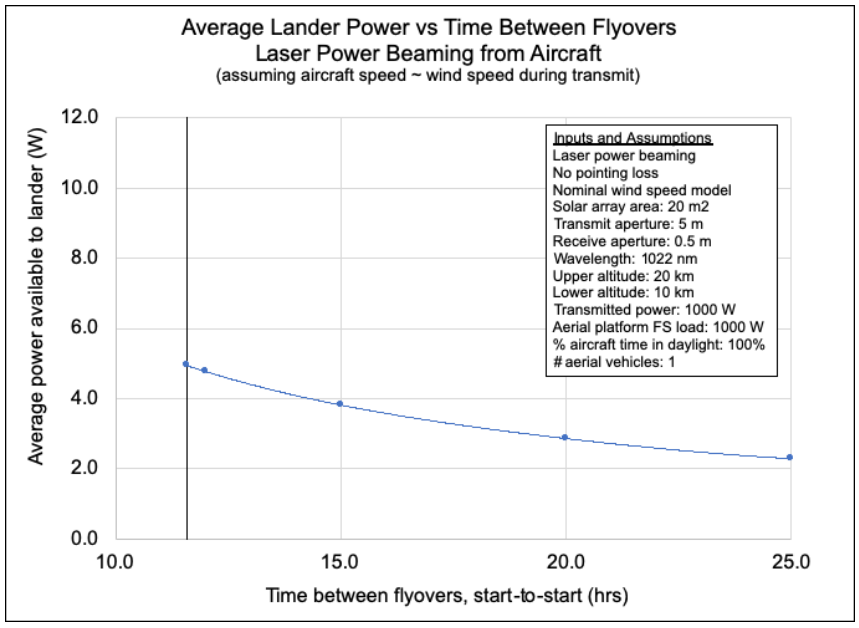

Fig. 26. Laser power beaming from aircraft. Average power available to the lander is plotted versus the time between flyovers. The aircraft returns to transmit power more quickly than the balloon.

TABLE 4. Lander Energy Balance – Aircraft Example

Parameter	Value	Comment
Transmitted power	1.0 kW	Input assumption
Average transmission efficiency during flyover	3.657%	Calculated in system model; includes atmospheric losses and LPC efficiency
Transmit duration	2.0 hours	Input assumption
Harness/diode efficiency	97%	Model input; accounts for resistive and blocking diode losses
Power system efficiency	90%	Model input; accounts for difference between battery voltage and optimum LPC voltage
Battery roundtrip efficiency	90%	Model input; based on Li(Al)-FeS battery
Available energy	57.5 Wh	Calculated from values above
Discharge duration	11.6 hours	Time needed to recharge the aerial battery, from Fig. 26
Average power available to lander	5.0 W	Available energy/discharge duration

4.4.2 Results for microwave power beaming from aerial platforms

Microwave power beaming was studied assuming transmission at frequencies from 1 to 94 GHz. Atmospheric attenuation severely constrained the candidate frequencies. As shown in Fig. 4, data from reference [33] show that atmospheric attenuation is very high at frequencies above 20 GHz. Below 20 GHz, beam spreading is the dominant factor.

The lowest practical altitude for power beaming was determined to be 10 km, due to the large variability in wind direction below this altitude. Hence, calculations were performed using the power system model assuming an altitude of 10 km and the data from reference [33]. As shown in Fig. 27, assuming 10 kW transmission, a 10 m transmitting aperture and a 10 m receiving aperture, the average power available to the lander from one aerial platform is still less than 0.1 W (-10 dBW). Therefore, it was concluded that microwave beaming would not be practical for power beaming to the surface of Venus.

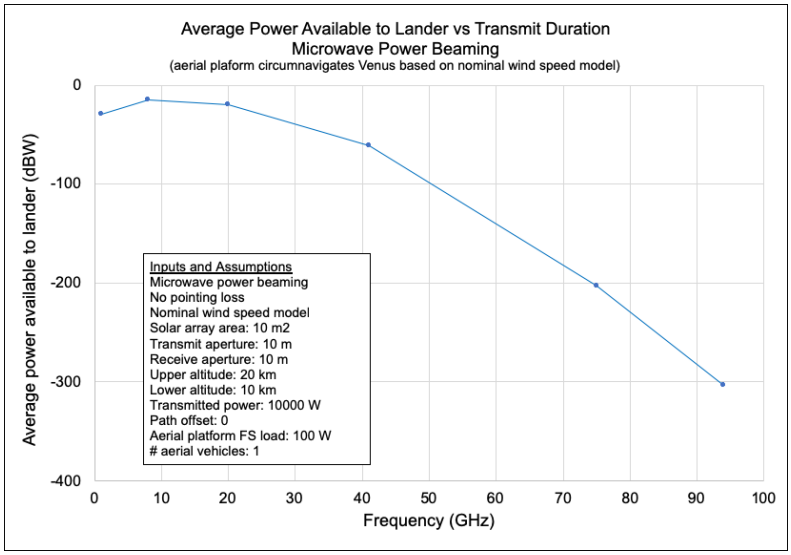

Fig. 27. Microwave Power Beaming from Balloon. Microwave power beaming does not appear to be practical at any frequency. Assuming 10 kW transmission, a 10 m transmitting aperture and a 10 m receiving aperture, the average power available to the lander from one aerial platform is still less than 0.1 W (-10 dBW).

4.4.3 Result for laser power beaming from orbiting platforms

The concept of an orbiting platform with a large solar array and high-power laser was considered. The orbiter would be in a circular orbit above the equator and would track the lander below when in view for laser power beaming. However, a cursory evaluation of the atmospheric losses showed that this approach is impractical. Specifically, the optical depth for the most favorable wavelength, 1022 nm, at 100 km is 30.6. This results in an attenuation of 4.9×10^{-14}. Hence, even a 100 kW laser at an altitude of 100 km directly above the target would provide only 4.9 nW at the surface. This is not enough power for even a single laser power converter to operate. Hence, it was concluded that laser power beaming from an orbiter would not be feasible.

5 Conclusions and Future Work

Candidate architectures were evaluated to enable power beaming to a lander on the Venus surface. Calculations showed that laser power beaming from a polymeric balloon is a viable option and is preferred over a metallic (lower altitude) balloon. Microwave power beaming does not appear feasible from any platform. Similarly, use of an orbiting platform does not appear feasible. Finally, laser power beaming is a promising alternative to microwave beaming, with options for transmission from either a series of balloons, or an aircraft. Although a balloon architecture may be possible, issues with pointing and control, combined with uncertainty over wind patterns make this option difficult to implement.

One of the prime advantages of an aircraft is that it possesses sufficient control authority (using standard aircraft control surfaces), to move between altitudes for alternately harvesting/beaming, as well as to stay on target for beaming to the lander. It would be preferable to implement a type of station-keeping flight pattern over the target, to avoid circumnavigation scenarios and maximize the beaming time to the lander (i.e., flying in a circular path over the lander, to maintain continuous pointing of the beaming laser to the laser power converter). Prior work [58,59] has indicated under certain conditions, a true solar powered aircraft could fly against the winds and maintain its position above a fixed landing site.

These earlier studies focused on aircraft flying at high altitudes (65+ km) and at high solar angles, to ensure sufficient availability of solar energy to power the propulsion system for station-keeping. This particular scenario was determined to be feasible. Further study is needed, however, to determine if the mission concept required to support flight for power beaming purposes can be achieved. Challenges include the aircraft descent (to sufficiently low altitudes to beam the power), followed by the climb back to the energy harvesting altitude. The winds are reduced at lower altitudes, however, the challenges of delivering sufficient aircraft power and selection of suitable high temperature materials remain, and will be studied further in Phase II.

The Phase II studies will leverage extensive prior studies in Venus aircraft (Fig. 28) [57-60]. As indicated above, a key extension to prior studies will focus on exploring aircraft capable of operating not just at the highest altitudes, but also at lower altitudes where the temperatures could reach $+300^{0}$C. Ultimately, the survival temperature may set the lower altitude at which the aircraft could beam power. The airframe, and methods for high temperature operation, would be evaluated in Phase II. For example, Blackswift Technologies has experience in the conceptual design of Venus aircraft and is the proposed lead for this feasibility study. This would include a high-fidelity simulation, using atmospheric models developed during a Phase I NASA Small Business

Innovative Research task. High temperature components (such as motors produced by Honeybee Robotics) would considered in the conceptual design activity.

A highly notional scheme for the overall mission concept is shown in Fig. 29 below, wherein an aircraft covered on its top and bottom surfaces with solar arrays and carrying suitable high temperature batteries and a laser beaming system 1) harvest solar energy at higher altitudes, potentially above the Venus cloud deck, 2) descend to a lower altitude, below the cloud deck but limited by the survival temperature of the aircraft structure and components, 3) beam continuously to the lander, while flying in a circular pattern above the landing site and finally 4) ascend to the higher altitude, to again harvest energy. Once the landed mission is completed (e.g., failure due to high temperature exposure), the aerial asset would have the opportunity to perform continued science investigations, assuming it outlives the lander. This overall mission concept, which builds on results from the Phase I study, will guide the Phase II study. The goal of this continued investigation remains the same: to provide adequate power for a long life Venus surface mission, to support a robust science investigation of this mysterious planet.

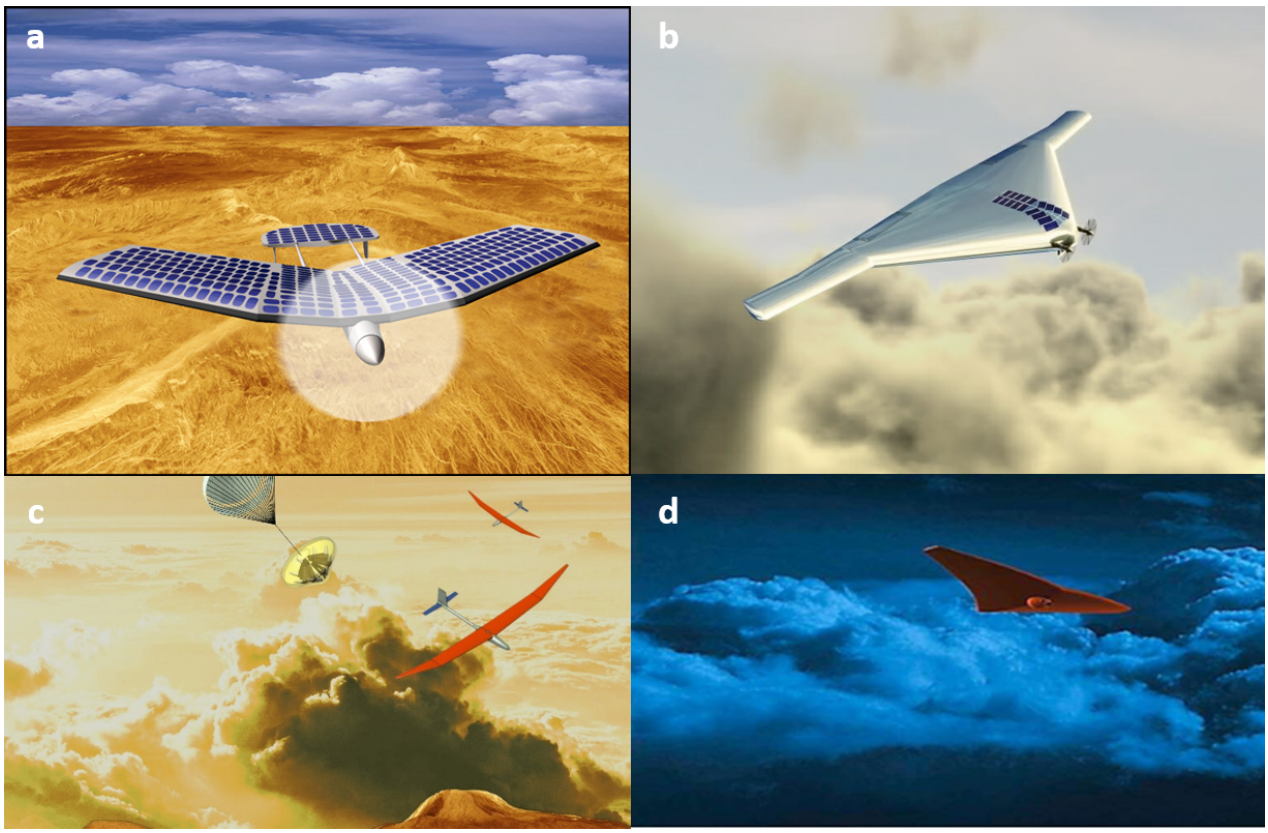

Fig. 28. Venus concept aircraft, including a a) solar airplane designed at NASA Glenn Research Center, b) Variable Altitude Maneuverable Platform (VAMP) designed at Northrup-Grumman, c) Dynamic soaring aircraft concept developed at BlackSwift Technology and d) Bioinspired Ray for Extreme Environments and Zonal Exploration (BREEZE) concept developed at the University of Buffalo.

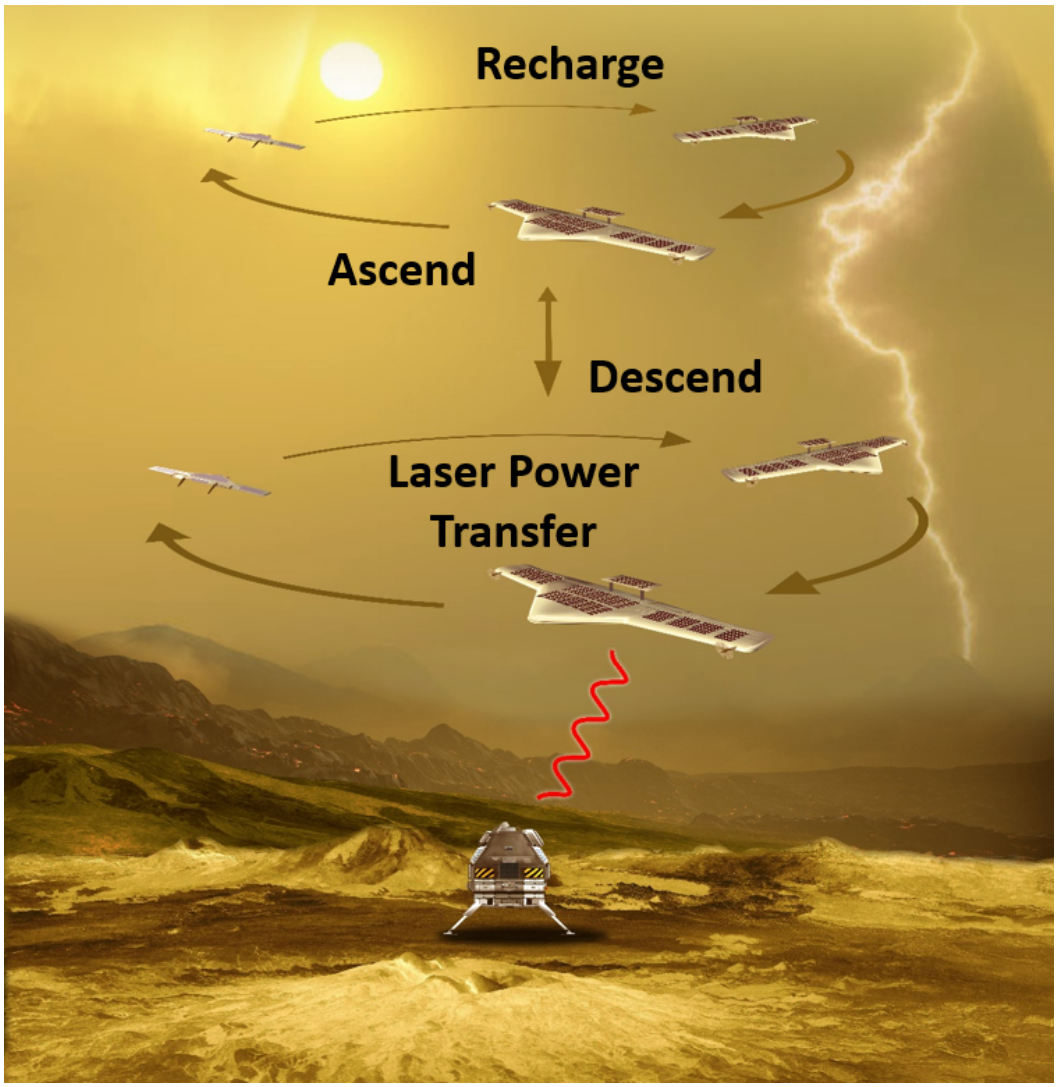

Fig. 29. Power beaming architecture concept, assuming a powered aircraft as the energy harvesting and beaming platform (power transmission using a laser beaming system). The feasibility of station-keeping flight patterns has been established at higher altitudes (65+ km), where solar energy is abundant. However, the feasibility of flying in this pattern at lower altitudes (and the maneuvers required to transition between altitudes) needs to be established.

6 REFERENCES

[1] J. O'Rourke, et al., 2019. Goals, Objectives, and Investigations for Venus Exploration, Venus Exploration Analysis Group.

[2] J. Hall, et al., 2009. Venus Flagship Study Report, Venus Science and Technology Definition Team.

[3] G. Hunter, et al., 2019. Venus Technology Plan, Venus Exploration Analysis Group.

[4] L. Zasova, et al., 2019. Venera-D: Expanding Our Horizon of Terrestrial Planet Climate and Geology Through the Comprehensive Exploration of Venus, Venera-D Joint Science Definition Team.

[5] T. Kremic, et al., 2017. Long-Life In-Situ Solar System Explorer (LLISSE) Probe Concept and Enabling High Temperature Electronics. Proc. of LPSC 48, The Woodlands, TX, Abstract #2986.

[6] T. Kremic, G. Hunter, J. Rock, P. Neudeck, D. Spry, G. Ponchak, J. Jordan, G. Beheim, R. Okajie, M. Scardelletti, J. Wrbanek, and J. Balcerski, 2018. Long-Lived In-Situ Solar System Explorer (LLISSE) probe development. Proc. of LPSC 49, Houston, TX, Abstract #2796.

[7] Q.V. Nguyen and G.W.Hunter, 2017. NASA High Operating Temperature Technology Program Overview, Proc. of 15th VEXAG Annual Meeting, Laurel, MD, Abstract #8046.

[8] G.A. Landis and R. Harrison, 2010. Batteries for Venus Surface Operation. J. Prop. Power, 26, 649-654.

[9] M.S. Gilmore, et al., 2010. Venus Intrepid Tessera Lander, Mission Concept Study Report to the NRC Decadal Survey Inner Planets Panel.

[10] M.L. Adams, et al., 2009. Venus Mobile Explorer, Mission Concept Study Report to the NRC Decadal Survey Inner Planets Panel.

[11] D.E. Glass, J.P. Jones, A.V Shevade, D. Bhakta, E. Raub, R. Sim, R.V. Bugga, 2020. High temperature primary battery for Venus surface missions, 449, 227492-1-227492-2.

[12] D. M. Hunten, L. Colin, T.M. Donahue and V.I. Moroz, 1983. Venus, University of Arizona Press, Tucson.

[13] V. I. Moroz, Y. M. Golovin, A. P. Ekonomov, B. E. Moshkin, N. A. Parfent'ev and N. F. San'ko, 1980. Spectrum of the Venus day sky, Nature, 284, 243-244.

[14] D. V. Titov, M. A. Bullock, D. Crisp, N. O. Renno, F. W. Taylor and L. V. Zasova, 2013. Radiation in the Atmosphere of Venus. In: L.W. Esposito, et al., Exploring Venus as a Terrestrial Planet, American Geophysical Union, 121-138.

[15] J. Grandidier, et al., 2019. Photovoltaic operation in the lower atmosphere and at the surface of Venus, Prog. Photovoltaics, https://doi.org/10.1002/pip.3214.

[16] V. I. Moroz, A. P. Ekonomov, B. E. Moshkin, H. E. Revercomb, L. A. Sromovsky, J. T. Schofield, et al., 1985. Solar and thermal radiation in the Venus atmosphere. Advance. Space Res., 5, 197-232.

[17] J. Grandidier, A. P. Kirk, M. L. Osowski, P. K. Gogna, S. Fan, M. L. Lee, et al., 2018. Low-Intensity High-Temperature (LIHT) Solar Cells for Venus Atmosphere. IEEE J. Photovoltaics, 8, 1621-1626.

[18] G.A. Landis and K.C. Mellot, 2010. Venus surface power and cooling systems, Acta Astronaut., 61, 995-1001.

[19] J. Sauder, 2017. Automaton Rover for Extreme Environments, NIAC Phase I Final Report.

[20] G.A. Landis, S.R. Oleson, T. Kremic, R.D. Patel, E.T. Reehorst and G.R. Hopkins, 2017. Small wind-powered missions to the surface of Venus. Proc. of AIAA Space and Astronautics Forum and Exposition, Orlando, FL, Paper AIAA 2017-5336.

[21] J. Sauder, B. Wilcox and J. Cutts, 2017. An Airborne Turbine for Power Generation on Venus. 15th Meeting of the Venus Exploration Analysis Group (VEXAG), Laurel, MD, Abstract #8037.

[22] R.D. Lorenz, 2016. Surface winds on Venus: Probability distribution from in-situ measurements, Icarus, 264, 311-315.

[23] T. Neuffer and S. Kremers, 2017. How wind turbines affect the performance of seismic monitoring stations and networks, Geophys. J. Int., 211, 1319–1327.

[24] M. Paul, A. Rattner and C. Greer, 2017. A Combustion-Driven Power Plant For Venus Surface Exploration, Proc. of LPSC 48, The Woodlands, TX, Abstract #2887.

[25] W.C. Brown, 1984. The History of Power Transmission by Radio Waves. IEEE Trans. Microw. Theory Tech., MTT032, 1230-1242.

[26] T. Shan and X. Qi., 2015. Design and optimization of GaAs photovoltaic converter for laser power beaming, Inf. Phys. Tech., 71, 144-150.

[27] R.A. Lower, G.A. Landis and P. Jenkins, 1995. Response of Photovoltaic Cells to Pulsed Laser Illumination, IEEE Trans. Electron. Dev., 42, 744-751.

[28] A. Celeste, P. Jeanty and G. Pignolet, 2004. Case study in Reunion Island, Acta Astronautica, 54, 253-258.

[29] N. Singh, C.K.F Ho, Y.N. Leong and K.E.K. Lee, 2016. InAlGaAs/InP-Based Laser Photovoltaic Converter at similar to 1070 nm, IEEE Electron. Dev. Lett., 37, 1154-1157.

[30] K. Jin and W. Zhou, 2019. Wireless Laser Power Transmission: A Review of Recent Progress, IEEE Trans. Power Electron., 34, 3842-3859.

[31] H. Brandhorst, 2018. Energizing the Future of Space Exploration: Applications of Space Solar Power, Proc. 6th IECEC, Cleveland, OH.

[32] E. Kolawa, et al., 2007. Extreme Environments Technologies for Future Space Science Missions, JPL Document D-32832.

[33] A. B. Akins, A. Bellotti, and P. G. Steffes, 2017. Simulation of the Atmospheric Microwave and Millimeter Wave Emission from Venus Using a Radiative Transfer Model Based on Laboratory Measurements, Venus Modeling Workshop, Cleveland, OH, LPI Contribution No. 2022.

[34] R. Haus, D. Kappel, and G. Arnold, 2015. Radiative heating and cooling in the middle and lower atmosphere of Venus and responses to atmospheric and spectroscopic parameter variations, Planet. Space Sci., 117, 262-294.

[35] T. D. Robinson and D. Crisp, 2018. Linearized Flux Evolution (LiFE): A technique for rapidly adapting fluxes from full-physics radiative transfer models, J. Quant. Spectrosc. Ra., 211, 78-95.

[36] Y. J. Lee, H. Sagawa, R. Haus, S. Stefani, T. Imamura, D. V. Titov, et al., 2016, Sensitivity of net thermal flux to the abundance of trace gases in the lower atmosphere of Venus, J. Geophys. Res. Planets, 121, 1737-1752.

[37] Y. J. Lee, K.-L. Jessup, S. Perez-Hoyos, D. V. Titov, S. Lebonnois, J. Peralta, et al., 2019. Long-term Variations of Venus's 365 nm Albedo Observed by Venus Express, MESSENGER, and the Hubble Space Telescope, AJ, 158.

[38] C. Kong, C. Pilger, H. Hachmeister, X. Wei, T. H. Cheung, C. S. W. Lai, et al., 2017. Compact fs ytterbium fiber laser at 1010 nm for biomedical applications, Biomed. Opt. Express, 8, 4921-4932.

[39] A. P. Ekonomov, V. I. Moroz, B. E. Moshkin, V. I. Gnedykh, Y. M. Golovin and A. V. Crigoryev, 1984. Scattered UV solar radiation within the clouds of Venus, Nature, 345-347.

[40] V. I. Moroz, A. P. Ekonomov, B. E. Moshkin, H. E. Revercomb, L. A. Sromovsky, J. T. Schofield, et al., 1985. Solar and thermal radiation in the Venus atmosphere, Adv. Space Res., 5, 197-232.

[41] M. G. Tomasko, L. R. Doose, P. H. Smith, and A. P. Odell, 1980. Measurements of the flux of sunlight in the atmosphere of Venus," J. Geophys. Res.-Space Phys., 85, 8167-8186.

[42] J. Cutts, D. Rodgers, J. Cameron, J. Hall, V. Kerzhanovich, E. Nilsen, et al., 1999. Venus Surface Sample Return: Role of Balloon Technology, AIAA International Balloon Technology Conference, Norfolk, VA.

[43] T.T. Yang, L. Cai and R.E. White, Mathematical modeling of the LiAl/FeS_2 high temperature battery system, J. Power Sources, 201, 322-331.

[44] J. L. Sudworth and A. R. Tilley, 1985.The Sodium Sulfur Battery, Chapman and Hall Ltd., England.

[45] X.C. Lu, J.P. Lemmon, V. Sprenkle and Z.G. Yang, 2010. Sodium-beta Alumina Batteries: Status and Challenges, JOM, 62, 31-36.

[46] J. L. Sudworth, 1994. Zebra batteries. J. Power Sources, 1994, 105–114.

[47] G. Li, X. Lu, J.Y. Kim, K.D. Meinhardt, H.J. Chang, N.L. Canfield, V.L. Sprenkle, Vincent, 2016. Advanced intermediate temperature sodium–nickel chloride batteries with ultra-high energy density, Nature Comm., 10683-1-10683-7.

[48] Y. Zhao, T. Palacios, 2019. High Temperature GaN Microprocessor for Space Applications, NASA HOTTech Review, August 21-22, 2019.

[49] C. Chapin, D.G. Senefsky, M. Rais-Zadeh, 2019. Passively Compensated Low Power Chip-Scale Clocks for Wireless Communication in Harsh Environments, NASA HOTTech Review, August 21-22, 2019.

[50] L. Del Castillo, W, West, T. Vo, T.Hatake, M. Mojrarradi, E. Kolawa, 2008. Extreme Temperature Sensing System for Venus Surface Missions, Proc. 2008 IEEE Aerospace Conference, Big Sky, MT.

[51] G. Hunter, 2019. Overview of HOTTech Integration Project and Long-Lived In-Situ Surface Explorer, NASA HOTTech Review, August 21-22, 2019.

[52] D. Makel, K. Baines, D. Pieri, G. Hunter, 2019. SiC Electronics to Enable Long-Lived Chemical Sensor Measurements at the Venus Surface. NASA HOTTech Review, August 21-22, 2019.

[53] R.D. Lorenz, 2015. Touchdown on Venus: Analytic Wind Models and a Heuristic Approach to Estimating Landing Dispersions, Planet. Space Sci., 108, 66-72.

[54] V. Kerzhanovich, J. Hall, A. Yavrouian and J. Cutts, 2005. Two Balloon System to Lift Payloads for the Surface of Venus, Proc. of AIAA 5th ATIO and 16th Lighter-Than-Air Sys Tech. and Balloon Systems Conferences, Arlington, VA, Paper AIAA-2005-7322. Arlington, Virginia, Sep. 26-28, 2005.

[55] Venus Aerial Platforms Study Team, 2018. Aerial Platforms for the Scientific Exploration of Venus, JPL D-102569.

[56] J.L. Hall, J.M. Cameron, M.T. Pauken, J.S. Izraelevitz, M.W. Dominguez, K.T. Wehage, 2019. Altitude-Controlled Light Gas Balloons for Venus and Titan Exploration, Proc. of AIAA Aviation Forum 2019, Dallas, TX, Paper AIAA 2019-3194.

[57] S. Warwick, F. Ross and D. Sokol, 2017. Venus Atmospheric Maneuverable Platform (VAMP) – Future Work and Scaling for a Mission, 15th Meeting of the Venus Exploration Analysis Group (VEXAG), Laurel, MD.

[58] G.A. Landis, C. LaMarre, and A. Colozza, 2005. Venus atmospheric exploration by solar aircraft, Acta Astronaut., 56, 750-75.

[59] G.A. Landis, A. Colozza, C.M. LaMarre, 2003. Atmospheric flight on Venus: A conceptual design, J. Spacecraft Rockets, 40, 672-677.

[60] K.L. Miller, 1995. Planetary Flight. J. Propul. Power, 11, 1063-1073.

7 ACRONYMS

AOI	Angle of Incidence
CV	Cyclic voltammetry
EQE	External quantum efficiency
fs	Femtosecond
JPL	Jet Propulsion Laboratory
LPC	Laser power converter
NASA	National Aeronautics and Space Administration
NIR	Near-infrared
rf	Radio frequency
RPS	Radioisotope power system
RTG	Radioisotope thermoelectric converter
VAMP	Venus Aerial Maneuverable Platform
VITAL	Venus Intrepid Tessera Lander
VEXAG	Venus Exploration Analysis Group
VME	Venus Mobile Explorer
YAG	Yttrium Aluminum Garnet
YDFL	Ytterbium-doped fiber lasers
ZEBRA	Zero Emission Battery Research Activities

8 ACKNOWLEDGEMENTS

The authors would like to thank Dr. Alex Akins of Georgia Tech, Dr. Yeon Joo Lee of the Technical University of Berlin and Dr. Dave Crisp of the Jet Propulsion Laboratory, for their support in modeling the interactions electromagnetic energy with the Venus atmosphere. We would also like to thank the NASA Advanced Innovative Concepts Program, for their sponsorship of this work. This work was partially carried out at the Jet Propulsion Laboratory, California Institute of Technology, under contract with the National Aeronautics and Space Administration.